The presence of Nd and Pr in HgMn stars

Dolk, Linus; Wahlgren, Glenn; Lundberg, Hans; Li, Zhongshan; Litzén, Ulf; Ivarsson, Stefan; Ilyin, I.; Hubrig, S.

[Link to publication]

Total number of authors:
8

The presence of Nd and Pr in HgMn stars

L. Dolk[1], G. M. Wahlgren[1], H. Lundberg[2], Z. S. Li[2], U. Litzén[1], S. Ivarsson[1], I. Ilyin[3], and S. Hubrig[4]

[1] Atomic Astrophysics, Department of Astronomy, Lund University, Box 43, 22100 Lund, Sweden
[2] Department of Physics, Lund Institute of Technology, Box 118, 22100 Lund, Sweden
[3] Astronomy Division, PO Box 3000, 90014 University of Oulu, Finland
[4] European Southern Observatory, Casilla 19001, Santiago 19, Chile

Abstract. Optical region spectra for a number of upper main sequence chemically peculiar (CP) stars have been observed to study singly and doubly ionized praseodymium and neodymium lines. In order to improve existing atomic data of these elements, laboratory measurements have been carried out with the Lund VUV Fourier Transform Spectrometer (FTS). From these measurements wavelengths and hyperfine structure (hfs) have been studied for selected Pr II, Pr III and Nd III lines of astrophysical interest. Radiative lifetimes for some excited states of Pr II have been determined with the aid of laser spectroscopy at the Lund Laser Center (LLC) and have been combined with branching fractions measured in the laboratory to calculate gf values for some of the stronger optical lines of Pr II. With the aid of the derived gf values and laboratory measurements of the hfs, a praseodymium abundance was derived from selected Pr II lines in the spectrum of the Am star 32 Aqr. This abundance was used to derive astrophysical gf values for selected Pr III lines in 32 Aqr, and these gf values were used to get a praseodymium abundance for the HgMn star HR 7775. The praseodymium abundance in HR 7775 was then utilized to derive astrophysical gf values for all observable Pr III lines in this star. The neodymium abundance, derived from unblended lines of Nd II in HR 7775, has been utilized to establish astrophysical gf values for observed Nd III lines in the optical region of this star. Selected Pr III and Nd III lines have been identified and studied in a number of HgMn stars and three hot Am stars. The praseodymium and neodymium abundance change rapidly from an approximate 1–1.2 dex enhancement for the hot Am stars to 1.5–3 dex enhancement for the cool HgMn stars, indicating a well-defined boundary between the hot Am and HgMn stars in the vicinity of 10 500 K. The enhancement of praseodymium and neodymium in Am and HgMn stars may be explained by diffusive processes active in the stellar atmosphere, while the observed discontinuity might be explained by a thin hydrogen convection zone thought to be present for the Am stars, but absent in the HgMn stars. The absence of a convection zone would cause the diffused elements to gather higher in the atmosphere of HgMn stars compared to Am stars, and explain the observed increase in abundance.

Key words. atomic data – stars: abundances – stars: chemically peculiar

1. Introduction

Noticeably strong spectral lines from singly-ionized rare earth elements (REE) ($Z = 57$–71)[1] are typically observed in the spectra of the cooler chemically peculiar (CP) stars (Am and Ap). As a result of the low ionization potentials of the REE, the hotter CP stars (including the HgMn and the Bp stars) have very weak or non-existent singly-ionized REE spectral lines. Instead, these stars should

have strong doubly-ionized lines for REE, provided that the elements are enhanced to a similar level as in the cooler CP stars.

In most hot Am and cool HgMn stars the Pr II lines are characteristically weak or absent, even though lines from both Ce II and Nd II may be readily observable (Cowley 1983). It is therefore thought that the praseodymium abundance is noticeably less than its even-Z neighbors, which might reflect the odd-even effect observed for the solar elemental abundance distribution among the lanthanides. The weakness or absence of the Pr II lines can be attributed to a combination of noticeable hyperfine structure (hfs) in the optical Pr II lines with the fact that REE lines from the doubly-ionized stage clearly dominate

---

[1] The rare earth elements are comprised of the lanthanides ($Z = 57$–71) and the actinides ($Z = 89$–103), but in the context of this paper we only consider the lanthanides as REE.

over singly-ionized lines in the temperature regime of the hot Am and HgMn stars when the abundance of praseodymium is sufficiently high to make the lines detectable. The third spectrum REE lines are thus a much better tool for investigating the REE abundances in the Am and HgMn stars.

Pr III lines were first observed in the HgMn star χ Lupi by Bidelman (1966). Guthrie (1985) noted the likely presence of Pr III in the HgMn star HR 7775, but did not find any evidence for Pr III lines in the other seven HgMn stars observed. Strong Pr III lines in HR 7775 were confirmed by Wahlgren et al. (2000) in the region around 5300 Å although an accurate abundance could not be determined due to the lack of oscillator strength data. In recent years it was noted that the third spectrum of praseodymium is very strong in some magnetic Ap stars (Mathys & Cowley 1992), even though the second spectrum is weak or absent.

In the present study, several cool HgMn stars have been observed primarily to search for lines from the third spectra of praseodymium and neodymium. The investigation was undertaken as part of a larger ongoing project investigating the presence and abundance of heavy elements in Am and HgMn stars and the presence of isotopic anomalies in elements with multiple stable isotopes. By looking for isotope anomalies in different elements, as well as abundance differences between lines originating from different ionization stages of one element, the study might also serve as a test of the diffusion hypothesis (Michaud 1970).

In this paper, selected Pr II and Pr III lines have been studied in order to provide information about wavelengths, atomic structure, and lifetimes for lines of astrophysical interest. Experimental lifetimes for selected levels of Pr II were obtained utilizing laser spectroscopic techniques, and gf values were calculated for lines of astrophysical interest. These experimental gf values were used to determine the praseodymium abundance in the Am star 32 Aqr. The praseodymium abundance was then used to determine astrophysical gf values for selected Pr III lines of this star. With the aid of these Pr III gf values the praseodymium abundance was calculated for the HgMn star HR 7775 (HD 193452). Astrophysical gf values were then determined for all observable Pr III lines in HR 7775, utilizing a larger spectral coverage (ranging from 3700 to 8000 Å).

Lines of Nd II with experimentally measured gf values have been utilized to derive a neodymium abundance in HR 7775. Using this abundance, as well as wavelengths of Nd III lines derived from known energy levels (Martin et al. 1978), several lines of Nd III have been identified and astrophysical gf values determined in HR 7775. The accuracy of the known Nd III energy levels were rather poor, which resulted in inaccurate values of the derived Ritz wavelengths. New laboratory measurements of Nd III were carried out with the Lund VUV FTS for accurate wavelengths.

Ultimately, with the newly determined astrophysical gf-values, the abundance and/or presence of praseodymium and neodymium are investigated for a number of cool HgMn stars. It is shown that the presence of these two rare earths is best studied via their third spectra where abundances in HgMn stars rival those determined from the second spectra for the cooler A type stars.

2. Observational data

The stars chosen for this study are mostly cool HgMn stars of spectral type B8-A0, primarily selected because the third spectrum of praseodymium had previously been observed in the two cool HgMn stars χ Lupi and HR 7775 (Wahlgren et al. 1994, 2000).

The main portion of the spectra were obtained with the 2.56 m Nordic Optical Telescope (NOT), located at the Roque de los Muchachos Observatory on the island of La Palma. The spectra were taken with the SOviet-FINnish (SOFIN) echelle spectrograph (Tuominen et al. 1998; Ilyin 1993, 2000) mounted at the Cassegrain focus. The SOFIN spectrograph is comprised of two optical trains, one of which provides access to a permanently mounted 1152×770 pixel array detector of camera focal length $f = 1000$ mm (camera 2), and one that provides access to a 1152×298 pixel detector for use with one of two interchangeable cameras of focal lengths $f = 2000$ mm (camera 1) and $f = 350$ mm (camera 3). The resulting resolving power for the three different cameras is wavelength dependent but is approximately $R = 170\,000$, $80\,000$ and $25\,000$ for cameras 1, 2 and 3, respectively. The wavelength coverage of camera 1 is approximately 14 Å per order for 10 to 12 orders, depending on the placement of the detector. Camera 2 provides twice the wavelength coverage per order for eight to 10 orders, while a camera 3 observation covers between 70 and 200 Å per order for approximately 38 orders. The sensitivity of the SOFIN spectrograph decreases towards the blue and the far red portions of the spectrum. In the present case most of the observations were made in the 5000 to 7000 Å region where the sensitivity is quite high. As a result the S/N ratios of the observations were mainly above 100:1.

The SOFIN observations were obtained mainly with the camera 2 setting, but several were also taken with camera 1. The resolving power for camera 2 is dependent on the placement of a line within an order, with the lines near the edge of an order displaying a significantly lower resolving power than the lines at the center of an order. To examine this effect the $FWHM$ was measured for a large number of lines in the Th–Ar comparison spectrum, and from these measurements a resulting resolving power was calculated. From these calculations it could clearly be seen that the resolving power at the edges of an order lies approximately at $50\,000$, after which it steadily increases towards the center of an order where it is around $85\,000$. It was subsequently shown that the increase in the resolving power towards the center of an order could best be described with a second order polynomial. As a further test similar calculations were made for several different

detector placements after which it was found that the resolving power only changes within an order and not from order to order.

The NOT/SOFIN spectra were obtained at two different grating settings, both placed within the visible portion of the spectral region between 4700 and 6500 Å (the stars HR 7775 and 32 Aqr were also observed at additional grating settings). The settings were selected to include unblended strong Pr III and Nd III lines previously observed in HR 7775. The observations at the two settings were obtained with camera 1 and camera 2, and many of the stars were observed with either both cameras and/or at both settings. Thus, the amount of data that were obtained varies from star to star.

Spectra of stars of interest to this program were also incorporated from observing programs run at the ESO 1.4 m CAT telescope and the CES Very Long Camera equipped with CCD Loral \#38 and at the ESO NTT 3.5 m telescope and the ESO Multi Mode Instrument (EMMI), both located at La Silla, Chile. Data were obtained at the CAT for the stars HR 6520, HR 6759 and HR 7245 during the time period 1998 July 25–August 1, and were reduced in a normal manner using MIDAS software. The CAT spectra were taken with the CES Long Camera, and were limited in wavelength to the interval 6130–6158 Å. Data quality is quite good, as defined by both high resolving power ($R \simeq 135\,000$) and signal-to-noise ratio ($S/N > 200:1$). Since these spectra were taken for other purposes the instrument setup is not optimal for searching for lines from the Pr III and Nd III spectra, and only a single Nd III line can be studied from these data. The NTT spectra cover a much larger wavelength interval (4070–6740 Å) at a resolving power of $R \sim 70\,000$ at $S/N \sim 100:1$. Data obtained for the stars χ Lupi, κ Cnc and HR 1800 were taken using the EMMI echelle spectrograph.

3. Laboratory analyses

3.1. Praseodymium

3.1.1. Wavelengths and atomic structure

The odd-Z ($Z = 59$) lanthanide praseodymium has only one stable isotope ^{141}Pr with a large nuclear spin ($I = \frac{5}{2}$) and nuclear magnetic moment ($\mu/\mu_{\mathrm{N}} = 4.136$). The low levels of Pr II belong to the configurations $4\mathrm{f}^3 6\mathrm{s}$ and $4\mathrm{f}^3 5\mathrm{d}$, and the lines that may be observed in stellar spectra are mainly transitions from these configurations to $4\mathrm{f}^3 6\mathrm{p}$. Due to the unpaired s-electron many of the $4\mathrm{f}^3 6\mathrm{s}$–$4\mathrm{f}^3 6\mathrm{p}$ lines exhibit large hyperfine structure, whereas the structure is considerably smaller in the $4\mathrm{f}^3 5\mathrm{d}$–$4\mathrm{f}^3 6\mathrm{p}$ lines. Improved wavelengths for selected Pr II lines in the region 2800–7900 Å that might be of astrophysical interest, as well as magnetic hyperfine constants for the involved 6s and 6p levels, have recently been measured by means of a Fourier transform spectrometer by the Lund University Atomic Astrophysics group (Ivarsson et al. 2001). The measurements also comprised branching fractions, which in combination with the lifetimes discussed below in

Sect. 3.1.2 were used for deriving oscillator strengths for Pr II lines.

In Pr III the ground configuration is $4\mathrm{f}^3$, and the lines likely to be observed in stellar spectra are $4\mathrm{f}^3$–$4\mathrm{f}^2 5\mathrm{d}$ transitions. As no unpaired s-electron is involved in the transitions, the hyperfine structure is small. The work by Ivarsson et al. (2001) also included accurate wavelength measurements of a number of strong Pr III lines, and in spite of the high resolution the hyperfine structure was only observed as a widening and an asymmetry of certain lines. Convolution of the FTS Pr III $\lambda5299.969$ line with Gaussian profiles of various resolution shows that line asymmetry starts to become noticeable in the line core for resolving powers near $R = 200\,000$. The lines are presented in Table 1, where the *FWHM* in Col. 3 shows the widening and the letter "v" in column one indicates the influence from the hyperfine structure.

As the *FWHM* is not an unambiguous measure of the width of an asymmetric line with a shoulder on one side, another measure of the influence of the hyperfine structure is shown in column two of the table. The column shows the ratio between the area of the Pr III line and the area of a single, unblended Pr II hyperfine component in the same region with the same peak intensity as the Pr III line.

The wavelengths, which correspond to the centers-of-gravity of the observed features, have an estimated uncertainty ranging from less than ±0.001 Å for the strongest lines to ±0.003 Å for the weakest.

3.1.2. Pr II lifetimes

Radiative lifetimes were measured for eleven levels in Pr II using laser spectroscopic techniques. In the experiment ions were created in a plasma produced by irradiating a praseodymium target with laser pulses. The measurements were performed close to the target during the plasma expansion. The ions were selectively photo-excited to the level under investigation by the light from a laser system in which pulses from a Nd:YAG laser were shortened in a stimulated Brillouin scattering (SBS) cell (Li et al. 1999) before pumping by a tuneable dye laser. Conventional Nd:YAG lasers produce pulses with a duration of about 10 ns and for precision in lifetime measurements the excitation pulse must be shorter than the investigated lifetime. The dye laser light could be shifted to desired wavelengths using frequency-doubling and Raman scattering. Fluorescence light released at the decay of the excited levels was captured using a fast detection system. The temporal shape of the laser pulse was also recorded and the lifetime values were evaluated by fitting a convolution of the recorded pulse and an exponential to the fluorescence.

The ground configuration in Pr II is $4\mathrm{f}^3 6\mathrm{s}$. Low lying levels of this configuration were used as a starting point for the laser excitation. In Table 2 the lower and upper levels are given (Martin et al. 1978) along with the excitation wavelengths relevant for these measurements.

Table 1. Laboratory wavelengths, widths and *FWHM* of strong Pr III lines.

Int.		$\dfrac{W_{\lambda,\mathrm{Pr\,III}}}{W_{\lambda,\mathrm{Pr\,II}}}$	$FWHM$ $(10^{-3}\ \mathrm{cm}^{-1})$	σ (cm^{-1})	λ_{air} (Å)	Classification
25		2.5	163	14055.845	7112.501	$4\mathrm{f}^3\ ^4\mathrm{I}_{11/2} - 4\mathrm{f}^2 5\mathrm{d}\ ^4\mathrm{K}_{13/2}$
157		2.2	126	14467.492	6910.126	$4\mathrm{f}^3\ ^4\mathrm{I}_{15/2} - 4\mathrm{f}^2 5\mathrm{d}\ ^4\mathrm{I}_{15/2}$
30		1.1	58	14906.337	6706.689	$4\mathrm{f}^3\ ^4\mathrm{I}_{15/2} - 4\mathrm{f}^2 5\mathrm{d}\ ^2\mathrm{I}_{13/2}$
22		1.3	66	15195.943	6578.871	$4\mathrm{f}^3\ ^4\mathrm{I}_{15/2} - 4\mathrm{f}^2 5\mathrm{d}\ ^4\mathrm{K}_{17/2}$
156		1.1	64	16135.955	6195.611	$4\mathrm{f}^3\ ^4\mathrm{I}_{9/2} - 4\mathrm{f}^2(^3\mathrm{H})5\mathrm{d}\ ^4\mathrm{H}_{7/2}$
167	v	2.6	145	16228.671	6160.215	$4\mathrm{f}^3\ ^4\mathrm{I}_{11/2} - 4\mathrm{f}^2(^3\mathrm{H})5\mathrm{d}\ ^4\mathrm{H}_{9/2}$
171	v	2.7	162	16415.819	6089.985	$4\mathrm{f}^3\ ^4\mathrm{I}_{13/2} - 4\mathrm{f}^2(^3\mathrm{H})5\mathrm{d}\ ^4\mathrm{H}_{11/2}$
72	v	3.2	289	16516.175	6052.981	$4\mathrm{f}^3\ ^4\mathrm{I}_{9/2} - 4\mathrm{f}^2 5\mathrm{d}\ ^4\mathrm{G}_{7/2}$
65	v	4.4	265	16665.040	5998.910	$4\mathrm{f}^3\ ^4\mathrm{I}_{11/2} - 4\mathrm{f}^2 5\mathrm{d}\ ^4\mathrm{G}_{9/2}$
176	v	2.8	180	16785.003	5956.035	$4\mathrm{f}^3\ ^4\mathrm{I}_{15/2} - 4\mathrm{f}^2(^3\mathrm{H})5\mathrm{d}\ ^4\mathrm{H}_{13/2}$
132		4.1	115	18721.350	5339.999	$4\mathrm{f}^3\ ^4\mathrm{I}_{15/2} - 4\mathrm{f}^2(^3\mathrm{F})5\mathrm{d}\ ^4\mathrm{H}_{13/2}$
1000	v	2.6	191	18862.748	5299.969	$4\mathrm{f}^3\ ^4\mathrm{I}_{13/2} - 4\mathrm{f}^2(^3\mathrm{F})5\mathrm{d}\ ^4\mathrm{H}_{11/2}$
735	v	1.4	123	18917.316	5284.681	$4\mathrm{f}^3\ ^4\mathrm{I}_{11/2} - 4\mathrm{f}^2(^3\mathrm{F})5\mathrm{d}\ ^4\mathrm{H}_{9/2}$
693		1.2	80	18990.076	5264.433	$4\mathrm{f}^3\ ^4\mathrm{I}_{9/2} - 4\mathrm{f}^2(^3\mathrm{F})5\mathrm{d}\ ^4\mathrm{H}_{7/2}$
282		1.3	97	19194.053	5208.487	$4\mathrm{f}^3\ ^4\mathrm{I}_{15/2} - 4\mathrm{f}^2 5\mathrm{d}\ ^2\mathrm{K}_{13/2}$

v denotes the line to be asymmetric with a shoulder on the short wavelength side.

Table 2. Measured Pr II levels and their lifetimes.

Level[a]	E_{exp} (cm^{-1})	Excitation Origin	$\lambda_{\mathrm{vac}}(\mathrm{nm})$	Conversion scheme	Observed fluorescence (nm)	Lifetime (ns) This Work Exp.	Previous Work Exp.
$4\mathrm{f}^3(^4\mathrm{I}^\circ)6\mathrm{p}\ ^5\mathrm{K}_5$	22 675.44	0	441.01	$2\omega+2\mathrm{S}$	441.0	13.0(1.1)	$15(1.5)^b$
$4\mathrm{f}^3(^4\mathrm{I}^\circ)6\mathrm{p}\ ^5\mathrm{K}_6$	24 115.50	441.95	442.41	$2\omega+2\mathrm{S}$	442.4	7.7(4)	$12(2)^b$
$4\mathrm{f}^3(^4\mathrm{I}^\circ)6\mathrm{p}\ ^5\mathrm{K}_7$	25 569.19	1649.01	418.06	$2\omega+2\mathrm{S}$	418.1	6.0(3)	$8.4(1.0)^b,\ 7.8(1.0)^c$
$4\mathrm{f}^3(^4\mathrm{I}^\circ)6\mathrm{p}\ ^5\mathrm{K}_8$	27 128.00	2998.36	414.43	$2\omega+2\mathrm{S}$	414.4	5.5(3)	$10(2)^b,\ 8.4(1.2)^c,\ 8.4(1.2)^d$
$4\mathrm{f}^3(^4\mathrm{I}^\circ)6\mathrm{p}\ ^5\mathrm{I}_6$	25 656.69	1649.01	416.53	$2\omega+2\mathrm{S}$	396.6	8.7(5)	$10(1)^b$
$4\mathrm{f}^3(^4\mathrm{I}^\circ)6\mathrm{p}\ ^5\mathrm{I}_7$	26 860.95	3403.21	426.30	$2\omega+2\mathrm{S}$	396.6	7.0(4)	$15(1.5)^b$
$4\mathrm{f}^2(^4\mathrm{I}^\circ)5\mathrm{d}\ ^1\mathrm{L}_8$	28 201.95	4437.15	420.79	$2\omega+2\mathrm{S}$	420.8	9.0(7)	$14(1)^b$
$4\mathrm{f}^3(^4\mathrm{I}^\circ)6\mathrm{p}?\ J=4$	24 745.95	441.95	411.45	$2\omega+2\mathrm{S}$	404.1	36(3)	
$4\mathrm{f}^3(^4\mathrm{I}^\circ)6\mathrm{p}?\ J=4$	25 467.47	1743.72	421.52	$2\omega+2\mathrm{S}$	399.6	12.4(1.1)	$13(1.5)^b,\ 9.5(1.5)^d$
$4\mathrm{f}^3(^4\mathrm{I}^\circ)6\mathrm{p}?\ J=5$	26 146.01	1743.72	409.80	$2\omega+2\mathrm{S}$	389.0	18.0(1.5)	
$4\mathrm{f}^3(^4\mathrm{I}^\circ)6\mathrm{p}?\ J=7$	28 009.80	1649.01	379.35	$2\omega+\mathrm{S}$	406.4	6.5(4)	$13(1.5)^b,\ 6.0(8)^c$

[a] Martin et al. (1978).
[b] Gorshkov & Komarovskii (1985).
[c] Andersen & Sörensen (1974).
[d] Andersen et al. (1975).

The blue wavelengths used for excitation can conveniently be produced by frequency-tripling an infrared Nd:YAG laser beam and let the produced UV beam pump a dye laser working with coumarine dyes. However, the pulse-shortening using SBS is performed in a water cell with green light, the second harmonic of the infrared. The short green pulses then pump a red dye, DCM, and the tuneable radiation is then frequency-doubled and Stokes shifted in a H_2 Raman cell. The conversion method is given in the fifth column of the table. In every conversion step pulse power is lost but the transitions are often saturated anyway and the pulse power then has to be further reduced using neutral density filters. In the measurements usually the strongest transition, selected by a monochromator, is used for detection and the transition starting from the lowest possible metastable level is used for excitation. The measured levels were chosen by identifying upper levels for transitions believed to be observable in stellar spectra and thus suitable for abundance determinations. The lifetime values are given in Table 2 together with results from previous measurements; Andersen et al. (1974, 1975) using the beam-foil technique and Gorshkow & Komarovskii (1985) employing electron beam excitation. For level and line-rich elements selectivity in both

excitation and detection is especially important. The band width of the laser light utilized in the present investigations was about 0.1 Å and the flourescent light was filtered by a monochromator. After setting the laser to the excitation wavelength for a level and observing fluorescence at an expected wavelength, a further test of proper level identifications was made in the measurements. The monochromator wavelengths were scanned in order to observe all the decay channels given for that level by the work of Corliss & Bozman (1962). For some levels in the list the agreement was too poor and lifetime measurements were not performed due to the uncertainty in level identification.

The advantage with a laser produced plasma as an ion source is the high ion density, the fairly high populations of metastable levels and the presence of high ionization stages. A major drawback is the high speed of the created ions. For Pr III this speed is on the order of 10 km s^{-1}. This puts constraints upon how long a lifetime can be measured. Attempts were made to measure the lifetimes for some of the lowest lying levels of Pr III, but the recorded decays in fluorescence were fitted poorly by the exponentials. During the recording the ions flew too long a distance which meant that some of them left the detection region before the de-excitation. The decay times were on the order of several hundreds of nanoseconds. The Pr III lifetimes could thus not be measured with any precision utilizing the employed technique. The problem can be reduced by using narrow band-width interference filters, selected for the relevant transitions, instead of a monochromator with a narrow slit.

3.2. Neodymium

Neodymium occurs in the form of seven stable isotopes, $A = 142, 143, 144, 145, 146, 148, 150$ with the relative terrestrial abundances 27%, 12%, 24%, 8%, 17% 6% and 6%. The odd isotopes thus represent 20% of the total abundance, and both isotope and hyperfine structure might be present in the spectral lines. The hfs will, however, generally not be observable, as the hfs patterns will be smeared out and completely masked by the components of the even isotopes. The isotopic shift is generally divided into mass shift and volume shift, where the former effect decreases and the latter increases with increasing mass through the periodic table. For neodymium the isotope shift is comprised of both mass and volume shift, but with the volume shift dominating (King et al. 1973). The volume shift is usually most prominent for configurations containing s-electrons.

The lowest even levels of Nd II belong to the $4f^4 6s$ and $4f^4 5d$ configurations. The odd parity upper levels in the transitions in the optical region are mainly from three configurations $4f^3 5d^2$, $4f^3 5d6s$ and $4f^4 6p$. Investigations have been made of the isotope shift of Nd II energy levels, the most extensive being that of Blaise et al. (1984), who measured the shift between the isotopes with masses $A = 144$ and $A = 150$ for over 300 energy levels, and

Nakhate et al. (1997) who measured the 144–150 shift for approximately 300 levels. In these studies the shift of the $4f^4 5d$ $^6K_{9/2}$ levels was defined as zero. The levels of the Nd II ground configuration $4f^4 6s$ show large isotope shifts due to the presence of the 6s electron, with a typical spacing between the $A = 144$ and $A = 150$ of 0.24 cm^{-1}, whereas the shifts of the $4f^4 5d$ levels are close to zero. The shifts of the odd levels involved in transitions in the optical region range from 0.15 to approximately 0.43 cm^{-1}, with the larger shifts being present for levels in the $4f^3 5d6s$ configuration.

Note should be made of the fact that the separation between the $A = 144$ and $A = 150$ isotopes of neodymium perhaps is not a good reflection of the observable isotope shift since the ^{150}Nd isotope is only responsible for approximately 6% of the total amount of neodymium in the terrestrial isotopic mixture, while approximately 88% of the isotopes are represented by the isotopes between $A = 142$ and $A = 146$. King et al. (1973) have measured isotope shifts between all the even isotopes for six spectral lines. In all of these the separation between the $A = 144$ and $A = 150$ isotopes is approximately twice as large as the separation between the $A = 142$ and $A = 146$ isotopes. Also, in measurements by Nöldeke (1955), Blaise (1957) and Ahmad & Saksena (1977), it can be noted that isotope shifts ^{144}Nd–^{150}Nd are approximately 3.4 times larger than the isotope shifts ^{142}Nd–^{144}Nd.

To conclude, the largest shift measured between the ^{144}Nd–^{150}Nd isotopes in a Nd II energy level is less than 0.5 cm^{-1}. A transition between such an energy level and a level without structure would result in a spectral line with a wavelength shift of approximately 0.1 Å in the optical region. This, coupled with the fact that the shift between the most abundant isotopes ^{142}Nd and ^{144}Nd is much smaller than the ^{144}Nd–^{150}Nd shift, means that the observed structure in Nd II lines is rather small, even in the most extreme cases. For these reason we have neglected Nd II line structure in the line lists used for making the synthetic runs for our abundance studies.

The gf values adopted for the observed Nd II lines are the experimental values from Meggers et al. (1975) and Ward et al. (1985).

The lowest levels of Nd III belong to the $4f^4$ configuration, and the strongest lines are $4f^4$–$4f^3 5d$ transitions. The amount of published laboratory data for Nd III is very scant, and only a few energy levels are included in the compilation by Martin et al. (1978). No line lists have been published, and as the reported energy levels are only given with one decimal, it is not possible to derive sufficiently accurate wavelengths from the level values. For this reason laboratory measurements of Nd III have been carried out with the Lund VUV FTS and new wavelengths have been determined (Aldénius 2001). Measured wavelengths in the region 4625–6550 Å from that work are presented in Table 7.

The Nd III lines of Table 7 showed a small influence of the isotope effect, mainly visible as an unresolved shoulder with an area of 5–6% of the total line. Comparisons with

the known structure of Nd I lines showed that this shoulder is caused by the ^{150}Nd isotope.

4. Spectrum analysis

Elemental abundances and astrophysical gf values were determined by comparing the observed spectra to synthetic spectra generated with the SYNTHE (Kurucz & Avrett 1981; Kurucz 1993a) program. Atomic line data were taken from the lists of Kurucz (1993a). Several of the lines studied for this paper were not present in the linelists. These lines, as well as hyperfine structure components, were individually entered into the linelists.

Before being fitted with synthetic spectra, the observational data were flux normalized to the line-free continuum level. The normalization procedure was accomplished with the use of an Interactive Data Language (IDL) procedure that allows the user to choose locations in the spectrum that will serve as continuum points (Wahlgren 1996). The choices of these points are not limited by the flux values and they can therefore be chosen with the aid of synthetic spectra. The normalization task was made easier by the fact that most of the observations were carried out in the red portion of the spectrum, where the line density is low and the continuum level is easily identified in the hot stars observed for this study. The uncertainty level for abundances resulting from improper continuum placement is dependent upon the observed S/N level. We estimate that for $S/N = 100$, the error in continuum placement is approximately 1% which, for example, results in an uncertainty of ± 0.05 dex in the abundance determined from the Pr III $\lambda 5264$ line.

The temperature range of HgMn stars is such that the majority ionization state of the praseodymium and neodymium atoms is doubly ionized. Until recently no oscillator strength data existed for Pr III or Nd III, making it impossible to directly determine an abundance from the third spectrum lines of these elements. Recently theoretical oscillator strength data have been made available both for Pr III (Palmeri et al. 2000; Bord 2000, private communication, Biémont et al. 2001) and Nd III (Bord 2000).

The complexity of the Pr III and Nd III spectra coupled with the nature of theoretical oscillator strengths means that any uncertainties attached to the abundance determinations based upon these values must be tested. In order to circumvent this problem we have chosen to determine abundances directly from a star where both singly-ionized praseodymium and neodymium lines with known experimental oscillator strengths, as well as doubly-ionized praseodymium and neodymium lines, are visible. In this way the singly-ionized lines can be utilized to derive an abundance, grounded in experimentally determined f-values, that can be used for determination of astrophysical gf values for Pr III and Nd III lines. The astrophysical gf values can then be compared with the theoretical gf values to establish the reliability of these values, and be used as an abundance determining tool for the hotter HgMn stars, where the Pr II and Nd II lines are too

weak to be observed. An implicit assumption of this approach is that statistical equilibrium results in an unique abundance for all ions of an element. The validity of this assumption can be questioned since ionization anomalies and abundance stratifications have been reported for certain elements in HgMn stars (i.e. for mercury in Proffitt et al. 1999). So far, however, no note has been made of a REE ionization anomaly in these stars, although this might reflect errors in atomic data and difficulties in observing lines from multiple ionization stages.

4.1. 32 Aqr

The metallic-lined (Am) star 32 Aquarii (HD 209625 = HR 8410) is a slowly rotating single-lined spectroscopic binary. It was chosen as a target because it had been observed to have lanthanide overabundances (Magazzu & Cowley 1986) and since its $T_{\rm eff}$ is low compared to those of the HgMn stars observed for this study. It was therefore expected that lines from both the singly and doubly-ionized stages for praseodymium and neodymium would be visible in the spectrum.

Several elemental abundance analyses of 32 Aqr exist in the literature. Smith (1971, 1976) and Lane & Lester (1987) analysed 32 Aqr as part of larger studies of Am stars. The stellar parameters derived in the latter study were $T_{\rm eff} = 7300$ K, $\log g = 3.3$, $v \sin i = 19$ km s^{-1}, $\xi_{\rm turb} = 2.5$ km s^{-1}. Kocer et al. (1987) derived similar values for the stellar parameters with the exception of the microturbulent velocity, which was found to be $\xi_{\rm turb} = 4.5$ km s^{-1}.

In a more recent study (Bolcal et al. 1992) the determination of the temperature and surface gravity was made by comparing the values calculated in three different studies, two of which being the studies listed above (Lane & Lester, and Kocer et al.). The third set was determined by using the photometric relations of Moon & Dworetsky (1985) and the $uvby\beta$ photometry of Hauck & Mermilliod (1980). The effective temperature and surface gravity determined with this method were $T_{\rm eff} = 7870$ K, $\log g = 3.77$. The rotational velocity was measured to be $v \sin i = 5$ km s^{-1} by fitting Gaussian profiles to metal lines. This value is quite different from the value of $v \sin i = 19$ km s^{-1} listed by Hoffleit & Jaschek (1982). An elemental abundance analysis for 32 Aqr made by Adelman et al. (1997) showed that some of the Pr II and Nd II lines were appreciably strong. Subsequent synthetic spectrum calculation made by us prior to making observations showed that the strongest Pr III and Nd III lines should be observable in a star with a temperature and abundances corresponding to that of 32 Aqr, making it a suitable object to be used in our study.

The strong spectral lines in 32 Aqr are extremely asymmetric with depressed blue line wings, while the weaker lines appear to be symmetric. The large difference in line shapes between the strong and weak features makes it impossible to get a consistent fit to all spectral lines with a

single atmospheric model. The asymmetry of the strong lines has been interpreted by Landstreet (1998) as evidence for atmospheric velocity fields in 32 Aqr. According to Landstreet the standard assumption of a height independent microturbulent velocity field is not valid in at least some of the Am stars with $T_{\rm eff}$ around 8000 K. In these type of stars a variation of the microturbulent velocity with height has to be incorporated in order to improve the agreement between the observed and calculated line profiles.

The asymmetric line profiles of the stronger spectral lines in 32 Aqr make the determination of the atmospheric parameters more difficult. The values of elemental abundances and the turbulent velocity that we adopted for 32 Aqr in this paper are to some extent based upon values obtained from previous studies. The effective temperature and gravity were, however, calculated from the $uvby\beta$ photometric colours provided by Hauck & Mermilliod (1980). The rotational velocity was determined from synthetic line profile fitting to weak symetrically shaped spectral lines. The final values adopted for 32 Aqr were: $T_{\rm eff} = 7700$ K, $\log g = 3.65$, $v \sin i = 5$ km s^{-1} and $\xi_{\rm turb} = 4.0$ km s^{-1}.

4.2. HR 7775

HR 7775 (= HD 193452 = β^2Cap, $m_v = 6.10$, B9.5 III-IVp Hg) is a slowly rotating ($v \sin i = 2$ km s^{-1}) HgMn star. It is a visual binary to the bright star HR 7776 (= HD 193495 = β^1Cap), with a separation of 205 arcsec (Hoffleit & Jascheck 1982). HR 7775 and HR 7776 each have either confirmed or suspected companions. In the case of HR 7775 a binary component has been detected by the lunar occultation method, at a separation of 0.28 arcsec (Radick & Lien 1980). The magnitude difference between the two components is 3.05 magnitudes in the Stromgren b filter. The astrometric satellite *Hipparcos* detected HR 7775 as a binary with a separation of 0.68 arcsec and magnitude difference of 2.98 mag (Perryman et al. 1997). It is difficult to estimate if the secondary contributes to our spectrum of HR 7775 since the orbit of the secondary has not yet been determined. The contribution of the secondary to the spectrum is determined by the separation of the components at the time of the observation, their position relative to the slit, the slit width, and the seeing. Of these factors only the last two are known with any certainty (the slit width of the SOFIN camera 2 is 0.7 arcsec, and the seeing is typically sub arcsec), making it impossible to determine the contribution of the secondary to the light from HR 7775. In a case where both stars appear on the slit at the time of the observation a contribution of 6% is calculated from the observed magnitude difference for saturated lines. There is, however, no evidence for the presence of spectral lines from the secondary at the level of the noise, typically at the 1% level. In the present work, as in the work by Wahlgren et al. (2000) which shared the use of some of the spectra presented in this study, a possible contribution to the

spectrum of HR 7775 from the binary component was neglected as synthetic calculations showed that such a contribution would likely be very small, with a total contribution to the spectral continuum at the level of 2% altering abundances of the primary star by up to 0.07 dex. Thus, the introduction of a secondary could introduce larger errors than it would hope to reduce.

HR 7775 has previously been analysed by Adelman (1994) and Wahlgren et al. (2000) in the optical region, and by Smith & Dworetsky (1993) in the ultraviolet. The atmospheric parameters and elemental abundances for HR 7775 are derived from the previous works. The stellar parameters adopted in this work were $T_{\rm eff} = 10\,750$ K, $\log g = 4.0$, $v \sin i = 2$ km s^{-1}, and turbulent velocity $= 0$ km s^{-1}, as used by Wahlgren et al. (2000).

The factors low-rotational velocity, enhanced line strengths for heavy elements, and its well studied nature made HR 7775, along with 32 Aqr, a prime target for the determination of astrophysical gf values for lines of Pr III and Nd III. The neodymium abundance in HR 7775 turned out to be sufficiently enhanced for lines from both Nd II and Nd III to be visible. Therefore, the Nd II lines were used for abundance determination, which in turn was used for the determination of astrophysical gf values for Nd III lines. The astrophysical gf values were determined using the implicit assumption that no ionization anomaly exists for neodymium (and praseodymium) in HR 7775 and for praseodymium in 32 Aqr, even though there is no direct evidence against REE ionization anomalies in these stars. Wahlgren et al. (2000) noted that some elements in HR 7775 have slightly different abundances when derived from lines of different ionization stages. These differences are generally small enough (0.1–0.2 dex) that they can be explained by errors in gf values, uncertainties in the line fitting procedure or lineblending.

There are some clues that an anomaly, if present, should be quite small for neodymium in HR 7775 and 32 Aqr. One such clue is that the astrophysical gf values of selected Nd III lines in 32 Aqr and HR 7775 agree very well. Since both sets of values were determined from the abundance derived from Nd II lines, this implies that both stars lack an ionization anomaly for neodymium, or that both stars have a similar anomaly. Since the two stars are different in temperature and chemical composition, there is no reason to believe that they should have a similar anomaly. For praseodymium a similar comparison can not be made due to the weakness of the Pr II lines in HR 7775. However, astrophysical gf values calculated from the upper limit abundance from Pr II lines agree very well with the astrophysical gf values determined from 32 Aqr. Another indication of a lack of a significant ionization anomaly is that praseodymium and neodymium abundances derived from lines from the first and second ionization stages were compared for a sample of magnetic and non-magnetic CP stars in the paper by Ryabchikova et al. (2001), and it was found that all of the observed pulsating magnetic (roAp) stars and several of the non-pulsating Ap stars show a large ionization anomaly, while no anomaly was found for several

Ap stars, the two Am stars 15 Vul and 32 Aqr, and the HgMn star HR 7775. Since this study utilized theoretical gf values for the observed Nd III and Pr III lines an ionization anomaly could conceivably be masked by errors in the calculations. However, this would mean that several very different stars would have a similar ionization anomaly for praseodymium and neodymium, which would be a remarkable coincidence.

4.3. Program stars

The stars observed for this study were mainly cool and fairly bright HgMn stars with the constraint that the projected equatorial rotational velocities ($v \sin i$) were low enough (≤ 30 km s^{-1}) to alleviate blending problems and problems discerning weak spectral features.

HgMn stars as a group are among the most slowly rotating stars on the upper main sequence (Wolff & Preston 1978) and they display very low values of microturbulence (Adelman 1994), which are properties suggesting that their atmospheres are rather stable. The surface composition of HgMn stars is characterized by profound enhancements of many elements, as well as the depletion of others.

By utilizing published photometric data, solar abundance LTE models were calculated using the ATLAS9 model atmosphere program (Kurucz 1993b). Synthetic spectra were then created using the model atmospheres and the SYNTHE program (Kurucz 1993a), from which elemental abundances and $v \sin i$ were determined. For most stars elemental abundances had been determined previously in which case those values were used as starting values in synthesizing spectra.

The observed stars are listed in Table 3 together with spectral types from the catalogue of Renson (1991) and photometric parameters from Hauck & Mermilliod (1980). For the cases where the stars are listed in the literature (see for example Batten et al. 1989) or observed by us as spectroscopic binaries the designations SB1 and SB2 are given for single-lined and double-lined spectroscopic binaries. Of the 19 HgMn stars observed, 10 are listed as spectroscopic binaries, which is consistent with the observed frequency of 50% or higher for spectroscopic binaries in the class as a whole (Aikman 1976; Gerbaldi et al. 1985; Schneider 1986; Hubrig & Mathys 1995).

The three stars ν Cnc, ϕ Her and HR 7664, which are considered single-lined spectroscopic binaries (Batten et al. 1989; Abt & Snowden 1973; Aikman 1976), were treated as single objects in the synthetic spectrum analysis since no information is available about their secondaries. Furthermore, none of these stars show any clear signs of a secondary in our data.

HR 1800 has been observed by *Hipparcos* to be a binary with a V magnitude difference of 0.956 mag and a separation of 0.243 arcsec. At first glance, no clear signs of a secondary can be seen in the spectrum of HR 1800, even though the small magnitude difference and separa-

tion would suggest that light from the secondary should give a rather large contribution to the spectrum. By observing the Hβ line and Mg II $\lambda 4481$ doublet the presence of the secondary could clearly be seen as a depression in the continuum around these lines. The shallowness of the depression suggested that the rotational velocity of the secondary was quite high. With the aid of the observed magnitude difference, and using the assumption of the secondary as a main sequence star, a model atmosphere was created for the secondary with solar abundance values, $T_{\mathrm{eff}} = 8500$ K, $\log g = 4.0$, $v \sin i = 50$ km s^{-1} and the luminosity ratio $L_{\mathrm{A}}/L_{\mathrm{B}} = 4$.

The remaining five SB2 HgMn binaries in Table 3 are all quite well studied, and for each the atmospheric parameters for both the primary and the secondary have been established along with the luminosity ratio between the two components. For all five stars, except κ Cnc, lines from the secondary component were observed in our data and a wavelength separation between lines from the primary and the secondary was established and used in the synthetic spectra. For κ Cnc a wavelength separation of zero angstroms was adopted, since the rotational velocity of the secondary is quite high, and the synthetic spectrum calculations thus quite insensitive to the separation.

The three Am stars Sirius, HR 3383 and o Peg with $T_{\mathrm{eff}} \approx 10\,000$ K were observed in order to investigate the boundary between the the hot Am stars and the HgMn stars. These stars are well-studied, and the physical parameters for them were adopted from previous work.

The physical parameters of the observed stars with their secondary components are listed in Table 4. The temperatures and gravities for the single stars and the primary components in the binaries were calculated from a computer code provided by R. Napiwotzki (1999 private communication; Napiwotski et al. 1993), which is based upon the formalism of Moon & Dworetsky (1985), and the $uvby\beta$ photometric colours presented by Hauck & Mermilliod (1980). For the secondary components these parameters were either adopted from previous work or calculated from the observed magnitude difference between the components and by utilizing the assumption that the secondary is a main sequence star.

The rotational velocities were determined by synthetic spectrum fitting of unblended Fe II lines. The element iron has four stable isotopes, but only one is dominant for the terrestrial isotope mixture (^{54}Fe:^{56}Fe:^{57}Fe:^{58}Fe = 5.8:91.7:2.2:0.3). Thus, the line core is dominated by the ^{56}Fe isotope, and isotopic shift and hyperfine structure play a negligible role in line broadening. Most of the Fe II lines used have similar sensitivity to a magnetic field, making it impossible to investigate the possible presence and strength of a magnetic field. For this reason a possible contribution of a magnetic field to line broadening was neglected in the calculations of $v \sin i$. We note, however, that fitted line profiles do not seem distorted by potential Zeeman broadening, effectively limiting the presence of a noticeable global organized magnetic

Table 3. Spectral types and photometric parameters.

HD	Other identification	Spectral Type	binarity	V	$(b-y)$	m_1	c_1	H_β
35548	HR 1800	B9HgMn	SB2	6.57	-0.009	0.119	0.894	2.792
48915	Sirius A	A1		-1.46	-0.005	0.162	0.980	2.907
72660	HR 3383	A1		5.81	-0.010	0.163	1.057	2.886
77350	ν Cnc	B9SrCrHg	SB1	5.45	-0.018	0.131	1.007	2.814
78316	κ Cnc	B8MnHg	SB2	5.23	-0.040	0.115	0.558	2.717
89822	HR 4072	A0HgSiSr	SB2	4.93	-0.019	0.139	0.956	2.827
106625	γ Crv	B8HgMn		2.58	-0.044	0.108	0.756	2.717
129174	π Boo A	B9MnHg		5.00	-0.008	0.073	0.625	2.745
141556	χ Lupi	B9YHg	SB2	3.95	-0.020	0.129	0.948	2.841
143807	ι CrB	A0MnHg	SB2	4.98	-0.020	0.132	0.875	2.818
144206	υ Her	B9MnHg		4.76	-0.032	0.105	0.756	2.756
145389	ϕ Her	B9MnHg	SB1	4.27	-0.019	0.129	0.783	2.787
149121	28 Her	B9MnHgSr		5.65	-0.015	0.119	0.911	2.807
158704	HR 6520	B9MnHg		6.05	-0.020	0.117	0.577	2.757
165493	HR 6759	B8		6.20	-0.014	0.092	0.498	2.703
174933	112 Her	B9HgMn	SB2	5.48	-0.035	0.123	0.586	2.753
175640	HR 7143	A0HgMnY		6.21	$+0.001$	0.103	0.747	2.771
178065	HR 7245	B9HgMn		6.54	$+0.073$	0.077	0.729	2.718
186122	46 Aql	B9MnHg		6.30	-0.019	0.094	0.641	2.729
190229	HR 7664	B9HgMn	SB1	5.67	-0.041	0.102	0.599	2.695
193452	HR 7775	B9HgPtSr	SB1	6.10	-0.007	0.138	0.909	2.845
209625	32 Aqr	A4m	SB1	5.28	$+0.118$	0.252	0.917	2.820
214994	o Peg	A1		4.81	-0.005	0.151	1.108	2.854

field. The determined values of $v \sin i$ are listed in Table 4 along with previously determined values.

5. Results

5.1. Praseodymium in 32 Aqr and HR 7775

A number of very weak Pr II lines appear in the spectrum of HR 7775. The weakness of the lines renders a direct abundance determination difficult, and for most lines it is only possible to determine an upper limit of the abundance. The Am star 32 Aqr was considered a suitable target where temperature and high praseodymium abundance would combine to make lines of both Pr II and Pr III visible. Unfortunately, the praseodymium abundance stated in previous work (Magazzu & Cowley 1986) was apparently overestimated, which meant that the strength of the observed Pr II and Pr III lines was less than anticipated. However, the abundance was high enough so that some of the stronger lines from both ionization stages were visible, although quite weak. Only for Pr II $\lambda\lambda 4056$, 4062, for which we had determined experimental gf values and hyperfine component intensities, were the line structures relatively unblended and sufficiently strong. With the aid of synthetic spectra a satisfactory fit to both lines was obtained at an abundance of log $N_{Pr} = 1.60 \pm 0.15$ dex (on a scale where log $N_H = 12$). The uncertainty in the abundance determination was calculated by using synthetic spectra to determine the change in the abundance value for a plausible variation of each parameter independently. In the error analysis T_{eff} was changed by ± 200 K, log g by ± 0.3, $v \sin i$ by ± 0.5 km s^{-1}, ξ_{turb} by ± 1 km s^{-1}. The error caused by improper continuum

placement was accounted for by allowing it to change by $\pm 1\%$ from its determined placement. The quoted error is a calculated root sum squared (rms) value based on the individual uncertainties of the five parameters. This rms value was deemed appropriate to use as a representation error estimate for other abundance determinations as well as for the determination of astrophysical log gf values. Some error sources are not included in the rms value. The error associated with fitting the observation by the synthetic spectra is not included, but it is less than 0.05 dex. Similarly, errors arising from incorrectly determined laboratory gf values and from the inappropriateness of the stellar model in terms of diffusion (for example), have not been incorporated.

After the praseodymium abundance had been determined from Pr II lines with experimental oscillator strength data, astrophysical gf values were determined for the three Pr III lines in 32 Aqr for which data had been obtained. The gf values were obtained by adjusting this parameter until the calculated line profile agreed with the observed line profile. The uncertainty in astrophysical log gf for the three Pr III lines is estimated to be ± 0.15 dex, based upon the rms error discussed above. It should be noted that the three Pr III lines have a small amount of hfs in the laboratory data as indicated in Table 1. Since the hfs can only be seen as a skewness of the laboratory Pr III lines observed at a spectral resolving power of $R = 10^6$, it is difficult to establish the strength of the hfs components. Each Pr III line is therefore only represented by a single component.

The extreme asymmetry observed in the line profiles of the stronger spectral lines in 32 Aqr is not evident in

Table 4. Physical parameters of the observed stars.

HD		$T_{\rm eff}$	$\log g$	$v \sin i$ (km s^{-1})		Ref.
		(K)		this work	other work	
35548	A	11 088	3.79	2	1	[1]
	B	8500	4.00	50:		
48915		9850	4.30	16	15	[2]
72660		9750	4.00	6.5	6.5	[3]
77350		10 375	3.50	20	13	[4]
78316	A	13 470	3.81	6.5	6	[5]
	B	8500	4.00	40	40	[6]
89822	A	10 900	4.07	3	$\leq$2	[6]
	B	8900	4.20	5	$\leq$2	[6]
106625		12 002	3.31	36	36	[7]
129174		13 037	3.97	14	15	[8]
141556	A	10 608	3.98	0	0	[9]
	B	9200	4.20	2	2	[9]
143807	A	11 250	3.65	2.5	$\leq$0.5	[6]
	B	9250	4.00	3	$\leq$0.5	[6]
144206		12 013	3.73	11	11	[10]
145389		11 781	3.97	10	10	[11]
149121		10 908	3.83	8	8	[11]
158704		13 163	4.22	4	3.75	[12]
165493		13 890	3.90	3	2.75	[12]
174933	A	13 294	4.15	6	6	[13]
	B	8500	4.20	8	8	[13]
175640		12 077	3.92	2	2	[1]
178065		12 193	3.54	2	1.5	[12]
186122		12 914	3.74	2	1	[1]
190229		13 240	3.43	9	8	[11]
193452		10 750	4.00	2	2	[14]
209625	A	7700	3.65	5	19	[15]
214994		9590	3.60	8	10	[2]

References to previous $v \sin i$ determinations: [1] Smith (1992);
[2] Abt & Morrell (1995); [3] Nielsen & Wahlgren (2000); [4]
Adelman (1989); [5] Adelman (1987); [6] Ryabchikova (1998);
[7] Guthrie (1981); [8] Adelman (1992); [9] Wahlgren et al.
(1994); [10] White et al. (1976); [11] Adelman (1988); [12]
Hubrig et al. (1999); [13] Ryabchikova et al. (1996); [14]
Wahlgren et al. (2000); [15] Hoffleit & Jaschek (1982).

weaker spectral lines. The Pr II and Pr III lines are quite
weak in 32 Aqr and no asymmetry (except hfs in the
Pr II lines) can be seen in the observed features. The uncer-
tainty of the astrophysical log gf values should therefore
not be affected by a disagreement between the synthetic
and observed line profiles due to asymmetries in the ob-
served spectral lines.

With the aid of the astrophysically determined gf val-
ues for the three Pr III lines in 32 Aqr an abundance de-
termination was made for praseodymium in HR 7775. The
derived abundance was log $N_{\rm Pr} = +3.68$ dex for each of
the three lines, an indication that the derived gf values

are consistent. The abundance value is also consistent with
an upper limit value determined from Pr II lines.

The laboratory spectrum of Pr III has been studied
extensively by Sugar (1974). From this study it is evident
that the strongest Pr III lines lie between 5000 and 7000 Å
and have thus been overlooked by traditional abundance
analysis at blue wavelengths. All of the stronger lines in
this region of the laboratory spectrum, that is lines with
an intensity above 1000 on the laboratory scale presented
by Sugar, can readily be observed in the SOFIN spec-
trum of HR 7775. The intensity scale presented by Sugar
is wavelength dependent so that in more sensitive regions
(such as between 5000 and 5500 Å) lines with intensities
down to 100 can be observed, while in other regions, such
as above 6000 Å it can be difficult to observe lines with
intensities of 1000.

After establishing the praseodymium abundance in
HR 7775, astrophysical log gf values were determined
for 18 of the stronger, unblended lines of Pr III. Table 5
presents these data. The log gf accuracy for most lines is
estimated to be less than 0.1 dex, based upon the fitting
error of the synthetic line profile to the observed lines.
The correctness of the log gf value for $\lambda5208$ is some-
what doubtful since it is blended with Cr I $\lambda5208$, but
more importantly, since the strength of the line should be
much weaker according to the laboratory intensity mea-
surements made by Sugar. It is therefore conceivable that
this line is in fact blended with an unknown feature.

The wavelengths presented in Tables 1 and 5 differ
somewhat from those determined by Sugar (1974), typi-
cally by 0.02 Å. This difference is larger than the difference
in the listed measurement accuracies of the two projects.
In the present paper the center of gravity wavelengths of
the Pr III lines are presented.

The results for three sets of theoretical gf values are
also presented in Table 5. The three calculations were all
made utilizing the Cowan code (Cowan 1981), including
some relativistic effects in the optimization of the orbitals.
It is interesting to note that the theoretical values by Bord
(2000, private communication) and Biémont et al. (2001)
agree very well, while these values differ from those of
Palmeri et al. (2000) by about 1 dex. This suggests a
rather large systematic error in the theoretical gf values
by Palmeri et al.. Biémont et al. ascribed this difference
to a more realistic consideration of the core-polarization
effect in their calculations as opposed to the earlier work
of Palmeri et al.

For most lines the gf values determined by Bord and
Biémont et al. are in good agreement with the astrophysi-
cally determined values. Still, it is difficult to conclusively
state that these gf values are correct or to what extent
the gf values of Palmeri et al. are in error since system-
atic uncertainties may have been introduced for the as-
trophysically calculated gf values. The log gf values for
the Pr II lines used for the abundance determination are,
however, experimental, and are highly unlikely to be inac-
curate by 1 dex. According to diffusion theory, the abun-
dance of an element may differ noticeably when derived

Table 5. Atomic data for Pr III.

λ_{air} (Å)	Classification	Astrophysical log gf		Theoretical log gf			log N_{Pr}	
		32 Aqr	HR 7775	[1]	[2]	[3]	χ Lupi	HR 1800
5208.487	$4f^3\ ^4I_{15/2} - 4f^2(^3H)5d\ ^2K_{13/2}$		-1.00bl	-1.09	-1.14		2.85	
5261.678	$4f^3\ ^2K_{15/2} - 4f^2(^1I)5d\ ^2I_{13/2}$		-0.65	-0.72			2.90	
5264.433	$4f^3\ ^4I_{9/2} - 4f^2(^3F)5d\ ^4H_{7/2}$		-0.60	-0.59	-0.66	-1.62	2.80	2.50
5284.681	$4f^3\ ^4I_{11/2} - 4f^2(^3F)5d\ ^4H_{9/2}$	-0.50	-0.50	-0.51	-0.59	-1.55	2.80	2.45
5299.969	$4f^3\ ^4I_{13/2} - 4f^2(^3F)5d\ ^4H_{11/2}$	-0.20	-0.20	-0.45	-0.53	-1.49	2.80	2.45
5339.999	$4f^3\ ^4I_{15/2} - 4f^2(^3F)5d\ ^4H_{13/2}$		-0.60	-0.53	-0.61	-1.57	2.90	2.50
5844.413	$4f^3\ ^2H2_{9/2} - 4f^2(^3F)5d\ ^2G_{7/2}$		-0.75	-0.78	-0.85	-1.76	2.85	<2.50
5956.035	$4f^3\ ^4I_{15/2} - 4f^2(^3H)5d\ ^4H_{13/2}$		-0.60	-0.60	-0.70	-1.64	2.80	
5998.910	$4f^3\ ^4I_{11/2} - 4f^2(^3H)5d\ ^4G_{9/2}$		-1.40	-1.80	-1.80	-2.73	2.90w	
6052.981	$4f^3\ ^4I_{9/2} - 4f^2(^3H)5d\ ^4G_{7/2}$		-1.50	-1.91	-1.84	-2.78	2.80	
6089.985	$4f^3\ ^4I_{13/2} - 4f^2(^3H)5d\ ^4H_{11/2}$		-0.80	-0.69	-0.82	-1.76	2.80	2.50
6160.215	$4f^3\ ^4I_{11/2} - 4f^2(^3H)5d\ ^4H_{9/2}$	-0.90	-0.90	-0.82	-0.98	-1.91	2.75	2.45w
6195.611	$4f^3\ ^4I_{9/2} - 4f^2(^3H)5d\ ^4H_{7/2}$		-1.10	-0.86	-1.04	-1.97	2.85	
6866.801	$4f^3\ ^4I_{9/2} - 4f^2(^3H)5d\ ^4I_{9/2}$		-1.20	-1.32	-1.23	-2.18		
7030.388	$4f^3\ ^4I_{13/2} - 4f^2(^3H)5d\ ^4I_{13/2}$		-0.60		-0.78	-1.73		
7076.618	$4f^3\ ^4I_{11/2} - 4f^2(^3H)5d\ ^4I_{11/2}$		-0.85		-1.01	-1.96		
7426.475	$4f^3\ ^4I_{11/2} - 4f^2(^3H)5d\ ^2H_{11/2}$		-1.20		-1.40	-2.35		
7781.985	$4f^3\ ^4I_{9/2} - 4f^2(^3H)5d\ ^2H_{9/2}$		-1.20		-1.21	-2.16		

[1] Theoretical log gf values from Bord 2000 (private communication).
[2] Theoretical log gf values from the website `http://www.umh.ac.be/ astro/dream.shtml` following calculations in Biémont et al. (2001).
[3] Theoretical log gf values from Palmeri et al. (2000).
Notes: The designations "w" and "bl" denote the spectral line to be weak or blended.
Wavelengths in italics from the work by Sugar (1974).

from different ionization stages. There are, however, no clear signs of abundance differences on the order of 1 dex in any of the elements observed in HR 7775 for which two ionization stages have been observed, although ionization anomalies are seen to be as high as 0.5 dex (see Table 3 in Wahlgren et al. 2000).

5.2. Neodymium in 32 Aqr and HR 7775

In the spectrum of HR 7775 a number of Nd II lines are readily observable. The strongest attain a depth of 15% from the continuum level. Because of this, the determination of the neodymium abundance and the astrophysical gf values for Nd III lines could be done utilizing a more direct approach than for praseodymium. The appreciable strength of the Nd II lines in HR 7775 meant that the neodymium abundance could be determined directly for this star without using 32 Aqr as an intermediary object.

The neodymium abundance in HR 7775 was determined from a number of unblended and sufficiently strong Nd II lines, the gf values of which had been determined from three sources: Ward et al. 1985; Kurucz 1993a, as determined from lifetimes provided by Ward et al. 1985; and Meggers et al. 1975, corrected with a factor of 0.62 as given in Kurucz 1993a. In the present study 24 lines were observed and analyzed with synthetic spectra. The lines and

the abundance derived from them are presented in Table 6. From this table it can clearly be seen that an analysis of the different lines provide a similar abundance value. The one notable exception is the line at 4109.071 Å. The mean abundance value of neodymium in HR 7775, as derived from 20 unblended Nd II lines, is log N_{Nd} = +4.04 ± 0.12 dex. It might be argued that this abundance would be too high since no isotope and hyperfine structure components were used in the linelists of the synthetic calculations. The isotope structure in a specific line is less than 0.1 Å for the optical lines with the largest observed isotope structure, as calculated from the isotope structure of the Nd II energy levels (Blaise et al. 1984). In the laboratory measurements of neodymium, made with the Lund VUV FTS, a certain amount of structure can be seen in the Nd II lines observed in HR 7775. The structure is, however, very small in all these lines, and the lines can therefore be represented by a single component without introducing significant errors in the abundance determination. The spectrum of HR 7775 has a lower S/N (under 100) in the blue spectral region (roughly between 3700–4100 Å), which increases the uncertainty of the abundances derived from lines in this region.

An abundance determination of neodymium was also made for 32 Aqr with the aid of unblended Nd II lines. This analysis served to check the consistency of the abundance

Table 6. The abundance of Nd II in HR7775 and 32 Aqr.

λ_{air}[a] (Å)	log gf	Ref.	Classification[b]	log N_{Nd} 32 Aqr	HR 7775
3901.845	0.310	[1]	$4f^4(^5I)6s\ ^6I_{17/2} - 4f^4(^5I)6p\ ^6H_{15/2}$		4.00
3911.165	0.340	[1]	$4f^4(^5I)6s\ ^6I_{15/2} - 4f^4(^5I)6p\ 29362_{15/2}$		3.95
3951.142	0.010	[3]	$4f^4(^5I)6s\ ^6I_{11/2} - 4f^4(^5I)6p\ ^6I_{11/2}$		4.00bl
3963.105	0.160	[3]	$4f^4(^5I)6s\ ^6I_{15/2} - 4f^4(^5I)6p\ 29027_{17/2}$		4.10
4012.243	0.720	[3]	$4f^4(^5I)6s\ ^6I_{17/2} - 4f^4(^5I)6p\ ^6K_{19/2}$		4.25
4031.784	0.330	[1]	$4f^4(^5I)6s\ ^4I_{15/2} - 4f^4(^5I)6p\ 30781_{17/2}$		3.90
4059.951	−0.360	[1]	$4f^4(^5I)6s\ ^4I_{9/2} - 4f^4(^5I)6p\ 26274_{11/2}$	2.20	
4061.080	0.550	[3]	$4f^4(^5I)6s\ ^6I_{15/2} - 4f^4(^5I)6p\ ^6K_{17/2}$	2.25	4.05
4109.071	0.280	[3]	$4f^4(^5I)6s\ ^6I_{9/2} - 4f^4(^5I)6p\ 24842_{11/2}$	1.90	3.70
4109.448	0.300	[3]	$4f^4(^5I)6s\ ^6I_{13/2} - 4f^4(^5I)6p\ ^6K_{15/2}$	2.40	4.10
4133.351	−0.520	[2]	$4f^4(^5I)6s\ ^6I_{13/2} - 4f^4(^5I)6p\ ^6I_{11/2}$	2.40	
4156.078	0.200	[3]	$4f^4(^5I)6s\ ^6I_{11/2} - 4f^4(^5I)6p\ ^6K_{13/2}$		4.20
4177.320	−0.080	[3]	$4f^4(^5I)6s\ ^6I_{9/2} - 4f^4(^5I)6p\ ^6K_{11/2}$		4.10
4211.291	−0.720	[3]	$4f^4(^5I)6s\ ^4I_{9/2} - 4f^4(^5I)6p\ 25389_{9/2}$	2.25	
4232.374	−0.300	[3]	$4f^4(^5I)6s\ ^6I_{9/2} - 4f^4(^5I)6p\ 24134_{11/2}$		4.10
4284.509	−0.200	[3]	$4f^4(^5I)6s\ ^6I_{17/2} - 4f^4(^5I)6p\ ^6K_{17/2}$	2.45	
4303.571	0.140	[3]	$4f^4(^5I)6s\ ^6I_{7/2} - 4f^4(^5I)6p\ ^6K_{9/2}$		4.20
4358.161	−0.280	[3]	$4f^4(^5I)6s\ ^6I_{13/2} - 4f^4(^5I)6p\ ^6K_{13/2}$	2.45	4.10
4462.979	0.070	[2]	$4f^4(^5I)6s\ ^4I_{13/2} - 4f^4(^5I)6p\ ^6K_{15/2}$		4.10
5076.580	−0.250	[1]	$4f^4(^5I)6s\ ^4I_{15/2} - 4f^4(^5I)6p\ 25678_{17/2}$		4.00bl
5249.576	0.210	[2]	$4f^4(^5I)5d\ ^6L_{17/2} - 4f^4(^5I)6p\ ^6K_{15/2}$		4.05
5273.427	−0.120	[3]	$4f^4(^5I)5d\ ^6L_{13/2} - 4f^4(^5I)6p\ ^6K_{11/2}$		4.10
5293.163	−0.060	[2]	$4f^4(^5I)6s\ ^6L_{15/2} - 4f^4(^5I)6p\ ^6K_{13/2}$	2.50	4.15
5319.815	−0.210	[2]	$4f^4(^5I)6s\ ^6L_{11/2} - 4f^4(^5I)6p\ ^6K_{9/2}$		4.10
5688.518	−0.250	[3]	$4f^4(^5I)6s\ ^6K_{13/2} - 4f^4(^5I)6p\ ^6K_{13/2}$	2.40	

[a] Wavelengths from Kurucz 1993a, as determined from energy levels by Blaise et al. (1984)
[b] Classifications from Martin et al. (1978)
References: [1] Meggers et al. (1975), corrected with a factor of 0.62 as given in Kurucz (1993a); [2] Ward et al. (1985); [3] Kurucz (1993a), as determined from lifetimes provided by Ward et al. (1985).

determination for HR 7775 and to discern possible blends that could be present in HR 7775, while absent in 32 Aqr. The lower effective temperature of 32 Aqr results in the Nd II lines being stronger compared to the corresponding lines in HR 7775, even though the abundance enhancement is not nearly as pronounced as in HR 7775. This meant that certain lines which are too weak to be seen in HR 7775 could be used in the analysis. Nine lines were measured in 32 Aqr and are presented in Table 6. The neodymium abundance for 32 Aqr derived from these lines is log $N_{Nd} = +2.34 \pm 0.17$ dex.

Astrophysical gf values were determined for 20 Nd III lines and are presented in Table 7. To check the consistency of these gf values, the lines of Nd III which could be seen in the spectrum of 32 Aqr were also observed. In all cases, astrophysical wavelengths and gf values from the two stars were in good agreement with each other.

Theoretical log gf values have been calculated by Bord (2000) and are presented in Table 7. These values agree well with the astrophysical values for most lines, with some notable exceptions. The lines with the largest disagreement are weak lines (in HR 7775).

Since only a few energy levels, and thus few lines of Nd III are classified, it is conceivable that many other unidentified features in stellar spectra with neodymium enhancements could be attributed to Nd III, originating from unknown levels. This could partly explain the large number of unidentified lines for HR 7775 as noted by Wahlgren et al. (2000). Spectra taken with the Lund FTS confirm this as several lines that could be attributed to Nd coincide in wavelength with unidentified features in the spectrum of HR 7775.

5.3. Praseodymium and neodymium in HgMn stars

The neodymium and praseodymium abundance in HgMn stars was determined from Nd III and Pr III lines for which gf values had been astrophysically obtained. The specific lines that were observed varies since different stars

Table 7. Atomic data for Nd III.

| λ_{air}(Å) | | Classification | Astrophysical log gf | | Theoretical log gf^c | log $N_{\mathrm{Nd}}{}^d$ | |
Previous[a]	Recent[b]		32 Aqr	HR 7775		χ Lupi	HR 1800
4624.993	4624.9799	$4f^4\ ^5I_6 - 4f^3(^4I^o)5d\ J = 7$	-2.00	-2.05	-2.01	3.35	
4903.260	4903.2410	$4f^4\ ^5I_4 - 4f^3(^4I^o)5d\ ^5I_5$		-2.35	-1.86	3.30	
4921.024	4921.0431	$4f^4\ ^5I_6 - 4f^3(^4I^o)5d\ ^5I_7$		-1.80	-1.77	3.30	
4927.574	4927.4877	$4f^4\ ^5I_7 - 4f^3(^4I^o)5d\ J = 7$		-0.90	-0.86	3.30	2.90n
5085.001	5084.993[e]	$4f^4\ ^5I_6 - 4f^3(^4I^o)5d\ ^5I_6$		-1.80	-0.68	3.35bl	
5102.415	5102.4555	$4f^4\ ^5I_8 - 4f^3(^4I^o)5d\ ^5I_8$		-0.30	-0.40	3.35	2.80
5126.987	5127.0441	$4f^4\ ^5I_6 - 4f^3(^4I^o)5d\ ^5H_5$		-0.85	-1.09	3.40	3.00
5193.062	5193.0397	$4f^4\ ^5I_5 - 4f^3(^4I^o)5d\ ^5I_5$		-1.20	-0.77	3.20	2.90
5203.902	5203.9236	$4f^4\ ^5I_4 - 4f^3(^4I^o)5d\ ^5H_3$		-0.80	-1.19	3.35	2.95
5259.894	5259.8757	$4f^4\ ^5I_5 - 4f^3(^4I^o)5d\ ^5H_4$		-2.35	-1.15	3.40w	
5265.019	5264.9604	$4f^4\ ^5I_7 - 4f^3(^4I^o)5d\ ^5I_7$		-0.70	-0.67	3.30	2.90
5286.764	5286.7534	$4f^4\ ^5I_8 - 4f^3(^4I^o)5d\ J = 7$		-2.05	-1.60	3.40w	
5294.099	5294.1133	$4f^4\ ^5I_4 - 4f^3(^4I^o)5d\ ^5I_4$		-0.70	-0.67	3.35	2.95
5633.541	5633.5540	$4f^4\ ^5I_5 - 4f^3(^4I^o)5d\ ^5I_4$		-2.20	-2.01	3.40w	
5677.145	5677.1788	$4f^4\ ^5I_8 - 4f^3(^4I^o)5d\ ^5I_7$	-1.40	-1.40bl	-1.42	3.60bl	
5845.068	5845.0201	$4f^4\ ^5I_8 - 4f^3(^4I^o)5d\ ^5K_9$	-1.10	-1.10	-1.16	3.35	2.85n
5987.800	5987.6828	$4f^4\ ^5I_7 - 4f^3(^4I^o)5d\ ^5K_8$	-1.25	-1.15	-1.25	3.30	2.90n
6145.072	6145.0677	$4f^4\ ^5I_6 - 4f^3(^4I^o)5d\ ^5K_7$	-1.30bl	-1.30	-1.33	3.35	2.90n
6327.244	6327.2649	$4f^4\ ^5I_5 - 4f^3(^4I^o)5d\ ^5K_6$	-1.35	-1.35	-1.40	3.35	3.00
6550.326	6550.2314	$4f^4\ ^5I_4 - 4f^3(^4I^o)5d\ ^5K_5$		-1.30	-1.47		

[a] Wavelengths calculated from Nd III energy levels, Martin et al. (1978).
[b] Wavelengths measured with the Lund VUV FTS, Aldénius (2001).
[c] Theoretical log gf values from Bord (2000).
[d] Abundance determined using astrophysical log gf values from HR 7775.
[e] Astrophysically determined wavelength.

Notes: The designations "w", "bl" and "n" denote the spectral line to be weak, blended or noise affected.

Table 8. Equivalent width measurements of Pr and Nd.

| | T_{eff}(K) | | | | | | | | |
	6000	7000	8000	9000	10 000	11 000	12 000	13 000	
Pr II	26.6	15.3	4.9	0.49					1 dex enhancement
Pr III	4.2	9.9	10.3	4.7	1.8	1.0	0.84	0.78	
Nd II	40.6	28.2	12.9	1.8	0.19				
Nd III	8.4	17.3	19.5	11.4	5.3	3.2	2.6	2.5	
Pr II	39.6	27.7	12.4	1.4	0.14				1.5 dex enhancement
Pr III	10.6	20.9	22.4	12.2	5.3	3.1	2.5	2.3	
Nd II	56.2	40.7	25.6	5.0	0.57	0.09			
Nd III	17.7	30.5	33.3	24.6	13.5	8.8	7.4	6.9	
Pr II	56.0	39.8	25.0	4.3	0.4	0.08			2 dex enhancement
Pr III	21.4	34.3	36.2	25.5	13.6	8.6	7.1	6.6	
Nd II	84.1	54.5	38.7	12.7	1.7	0.3			
Nd III	30.2	43.0	48.2	38.4	27.0	19.5	17.1	15.7	

All equivalent widths measured in units of mÅ.

were observed with different spectrographs, modes, and wavelength intervals, and since the number of observable lines is dependant on the abundance of the element in question.

The strength of an individual neodymium or praseodymium line is not only dependant on the gf value and abundance, but also on the stellar effective temperature, through the Boltzman factor. Equivalent width measurements were made from synthetically calculated praseodymium and neodymium lines at different temperatures in order to investigate the temperature dependence of lines from different ionization stages. In the synthetic calculations the $\lambda5294$ line of Nd III and the $\lambda5299$ line of Pr III were used for the equivalent width measurements since these are among the strongest praseodymium and neodymium lines observed in HR 7775. To

compare lines from different ionization stages, theoretical singly and triply-ionized lines were created with the same $\log gf$ and energy level values as the doubly-ionized lines. Neutral lines were not studied since they display negligible strength in the temperature regime of the HgMn stars. Synthetic spectra were generated for atmospheric models with effective temperatures ranging from 6000 to 13 000 K at 1000 K intervals. The surface gravity in all models was $\log g = 4$. For each atmospheric model synthetic spectra were generated for neodymium and praseodymium abundance enhancements of 1.0, 1.5 and 2.0 dex. The equivalent width measurements for singly and doubly-ionized praseodymium and neodymium are presented in Table 8.

As evident from Table 8, the Pr II and Nd II lines have equivalent widths that decrease rapidly with increasing temperature. It is clear that lines from Pr II and Nd II should be very weak or absent in the temperature regime of the HgMn stars, even at a 2 dex abundance enhancement. Note should be made that while the strongest transitions in Pr II and Nd II have similar lower energy levels as the strongest Pr III and Nd III lines, they have substantially larger gf values. The astrophysically determined $\log gf$ value of the $\lambda5294$ Nd III and the $\lambda5299$ Pr III line is -0.7 and -0.2, respectively, while the strongest optical Pr II and Nd II lines have $\log gf$ values larger than $+0.5$. This means that measured equivalent widths are not representative of the strongest Pr II and Nd II lines, the equivalent widths of which should be noticeably larger. The strongest Pr II and Nd II lines might thus appear in the cooler HgMn stars, provided that the elements are sufficiently enhanced.

Table 8 shows that doubly-ionized praseodymium and neodymium becomes the dominant ionization stage, at an effective temperature below 8000 K. The lines of Pr III and Nd III decrease in strength with increasing temperature beyond 8000 K, but much less rapidly than the Pr II and Nd II lines. The temperature regime of the HgMn stars is thus not optimal for observing the Pr III and Nd III lines, but the slow decrease of the line strengths with temperature does imply that the lines should be observable in the HgMn stars, provided that the enhancement of the elements is sufficiently large.

The limit beyond which the equivalent width of a line becomes unobservable in a stellar spectrum is affected by the $v \sin i$ of the star and the signal-to-noise of the spectrum. In a high S/N, low $v \sin i$ spectrum we estimate the limit to be around 1 mÅ. From Table 8 it is seen that the equivalent width of the Pr III $\lambda5299$ line lies around 1 mÅ at a 1 dex enhancement of praseodymium in the temperature range of the HgMn stars. The Pr III line would thus be difficult to observe at this enhancement level under optimal conditions, and undetectable at low S/N and/or high $v \sin i$. Similarly, the line would be unobservable at an abundance enhancement less than 1 dex. The Nd III line has a 2–3 mÅ equivalent width at a 1 dex enhancement of neodymium, and should be observable at this enhancement level in less than optimum conditions.

Table 9. Observed Pr III lines in HgMn stars.

| Name | $\log N_{Pr}$ | | | | |
	$\lambda5284$	$\lambda5299$	$\lambda5340$	$\lambda5844$	$\lambda6160$
ν Cnc		2.10n	<2.70	<3.00	<2.80
χ Lupi	2.80	2.80	2.90	2.85	2.75
HR 7775	3.68	3.68	3.68	3.68	3.68
HR 4072		2.85	3.00bl	2.90n	2.90n
28 Her			2.70n		
HR 1800	2.45	2.45	2.50	<2.50	2.55
ι CrB		2.55	2.65	2.70n	2.65
ϕ Her	2.40bl	2.40	<2.70	<2.70	<2.60
γ Crv		<2.20n	<2.50n		
υ Her	<2.40n	2.20	2.30w		
HR 7143		<1.80n			
46 Aql			<1.90n		
π Boo A	<3.00bl	<2.70bl			<3.00w
HR 7664			<2.10		
112 Her			<2.40bl	<3.00w	<2.40
κ Cnc	<2.30bl		<2.30bl		

Notes: The designations "w", "bl" and "n" denote the spectral line to be weak, blended or noise affected.

The exclusion of equivalent width measurements of the Pr IV and Nd IV lines in Table 8 is motivated by the absence of any observable feature in the synthetic calculations at stellar effective temperature of 13 000 K and 2 dex enhancement. The ionization potential of Pr IV and Nd IV (38.94 and 40.4 eV) is evidently too large for lines from this ionization stage to present themselves in stellar spectra at effective temperatures below 13 000 K. Calculations show that the Pr IV and Nd IV lines are still absent in a star with an effective temperature of 25 000 K with this enhancement.

In Table 9 the calculated abundance of praseodymium, or the upper limit of the abundance, in the observed HgMn stars are presented for each of the observed Pr III lines. The uncertainty of the abundance determination varies from line to line as well as from star to star. In the cases where a specific line is strong and unblended, the error in the abundance determinations is estimated to be less than 0.1 dex. In several cases, however, lines are either blended, very weak, or affected by noise, in which cases the error in the abundance determination can be up to 0.2–0.3 dex.

The solar abundance of praseodymium is quite low, $\log N_{Pr} = 0.71$ (Grevesse et al. 1996), 0.54 (Ivarson et al. 2001), and a praseodymium enhancement of 1–2 dex (depending on $v \sin i$, S/N and T_{eff}) is needed in order to observe the strongest Pr III lines in the temperature regime of the HgMn stars. For this reason only an upper limit of the abundance can be found for several stars. Upper limits were established by increasing the abundance from the solar value until the synthetic line profile was outside the observed line profile.

Since the amount and quality of data varies from star to star some notes regarding the determined praseodymium abundance are presented for specific stars. For the stars ν Cnc and γ Crv the projected rotational

velocity is quite large ($v \sin i = 20$ and 36, respectively), which makes the determination of the abundance more problematic. In ν Cnc only the $\lambda5299$ line is useful for a direct abundance determination, all the other lines are only good for establishing a rather high upper limit. For the stars hotter than HR 7143 no praseodymium line can be observed with certainty, and only an upper limit of the praseodymium abundance can be established. The value of the upper limit established is clearly correlated to the $v \sin i$ of the star, with the slowly rotating stars having a much lower upper limit than those rotating more rapidly.

The cooler HgMn stars show greater abundance enhancement of praseodymium than the hotter ones. This is illustrated in Fig. 2 where the spectra of the Pr III $\lambda5299$ line is plotted for all HgMn stars where this line was observed. There is a feature at the same wavelength as the $\lambda5299$ Pr III line in 112 Her and κ Cnc, but the abundance value derived from this line is inconsistent with the praseodymium abundance derived from other Pr III lines. It is therefore believed that this feature originates from a transition in another element. No Pr III lines are observed with certainty in any of the observed HgMn stars with $T_{\text{eff}} > 12\,500$ K. The praseodymium abundance might still be enhanced, but not sufficiently for these Pr III lines to be observable.

The solar abundance of neodymium is low, $\log N_{\text{Nd}} = 1.50$ (Grevesse et al. 1996), yet higher than the praseodymium abundance. Since the strongest praseodymium and neodymium lines have similar $\log gf$ values, and originate from low energy levels, they should be equally strong provided that the abundance of the two elements is the same. We observe the neodymium abundance to be about 0.5 dex greater than the praseodymium abundance, which means the Nd III lines usually are stronger than the Pr III lines, and subsequently the neodymium abundance may be more easily determined than the praseodymium abundance.

The Nd III $\lambda5102$ line presented us with a problem. This line, which is the strongest of the observed Nd III lines in HR 7775, is blended with Mn II $\lambda5102$. In HR 7775 the manganese abundance is rather low for a HgMn star, and the Mn II line does not significantly blend with the Nd III line. In other HgMn stars the manganese abundance can be much higher and the effect of the Mn II line more prominent. It was noted that the abundance value derived from the $\lambda5102$ line of Nd III did not agree with the value derived from other Nd III lines whenever the manganese abundance was high enough ($\log N_{\text{Mn}} \geq 7.00$) for the blend to be substantial. For stars with solar-like manganese abundance the abundance derived from the Nd III $\lambda5102$ line agrees well with the abundance derived from other Nd III lines. This suggested that there was a problem with the Mn II line used in the synthetic calculations.

Manganese lines can show quite large hfs since manganese is an odd-Z element with a large nuclear spin ($I = \frac{5}{2}$) and magnetic moment ($\mu/\mu_N = 3.444$). The J values for the upper and lower energy levels of the Mn II
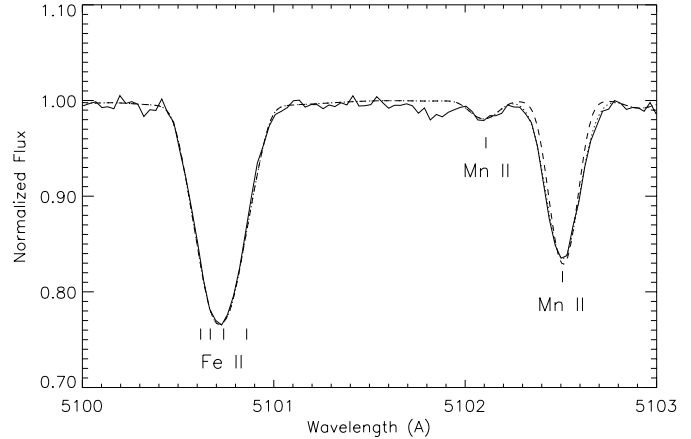
Fig. 1. Mn II $\lambda5102$ line. The original one component fit, represented by the dashed line, and the 16 component fit, represented by the dotted line, are compared to the observed spectrum (solid line) of κ Cnc. Four individual lines of Fe II comprise the anotated feature.

$\lambda5102$ line are both $J = 4.0$, and the line consists of 16 components. Measurements of hfs have been made for some Mn II lines (Holt et al. 1999), but not for the $\lambda5102$ line. To get a first approximation of the hfs of the $\lambda5102$ line the relative gf values of the $\lambda7110$ line measured by Holt et al., with the same upper and lower J values as the $\lambda5102$ line, were used. The relative gf values can as a first approximation be considered the same for the two lines. The wavelength spacing between the components may not be the same for the two lines, since the spacing depends on the magnetic dipole (A) and electric quadrupole (B) constants.

The HgMn star κ Cnc was utilized for the investigation of the hfs of the Mn II $\lambda5102$ line since no clear signs of a neodymium enhancement can be established from any of the other Nd III lines. The upper limit of the neodymium abundance in κ Cnc, as derived from other Nd III lines, is $\log N_{\text{Nd}} = 2.30$, and subsequent synthetic runs showed that this level of enhancement would affect the Mn II line only slightly. Several synthetic runs were made, all utilizing the relative gf values derived from the $\lambda7110$ line, but with different hyperfine splittings, until a good match was found between the observed and the synthetic line profiles. The resulting fit is presented in Fig. 1 along with the one component fit.

The 16 component representation of the Mn II line is useful for the purpose of determining the abundance from the blending Nd III line. A good indication of the validity of our approach is that the abundance derived from the Nd III $\lambda5102$ line agreed with that derived from other Nd III lines, even for the stars with large enhancement of manganese, after the inclusion of the hfs.

The Nd III $\lambda5294$ line is also blended with a Mn II line consisting of nine components, but the latter line is not broadened as much as the Mn II $\lambda5102$ line. This suggests that this Mn II line has a much smaller hfs splitting than the $\lambda5102$ line. In κ Cnc a one component synthetic fit

Table 10. Observed Nd III lines in HgMn stars.

Name				$\log N_{\mathrm{Nd}}$			
	$\lambda 5102$	$\lambda 5203$	$\lambda 5294$	$\lambda 5845$	$\lambda 5987$	$\lambda 6145$	$\lambda 6327$
ν Cnc	2.50		2.40	<3.00	<2.90	<2.90	<3.10
χ Lupi	3.35	3.35	3.35	3.35	3.30	3.35	3.35
HR 7775	4.10	4.10	4.10	4.10	4.10	4.10	4.10
HR 4072	3.55		3.55	3.50n	3.55	3.65n	
28 Her	2.65						
HR 1800	2.95	2.95	2.95	2.85	2.90	2.90	3.00
ι CrB	3.10		3.25	3.20	3.10	3.15	3.15n
ϕ Her	2.70	2.90bl	2.60	<2.90	<3.00bl	<2.90	
γ Crv	2.50n	2.40n	2.40n				
υ Her	2.50bl	2.50n	2.45bl				
HR 7143			<1.90				
HR7245						2.80n	
46 Aql	<1.90						
π Boo A	<2.60		<2.50				
HR6520						<3.10	
HR 7664	<2.00						
112 Her	<2.40n		<2.70n				
κ Cnc	<2.40	<2.20	<2.40				
HR6759						3.50	

Notes: The designations "w", "bl" and "n" denote the spectral line to be weak, blended or noise affected.
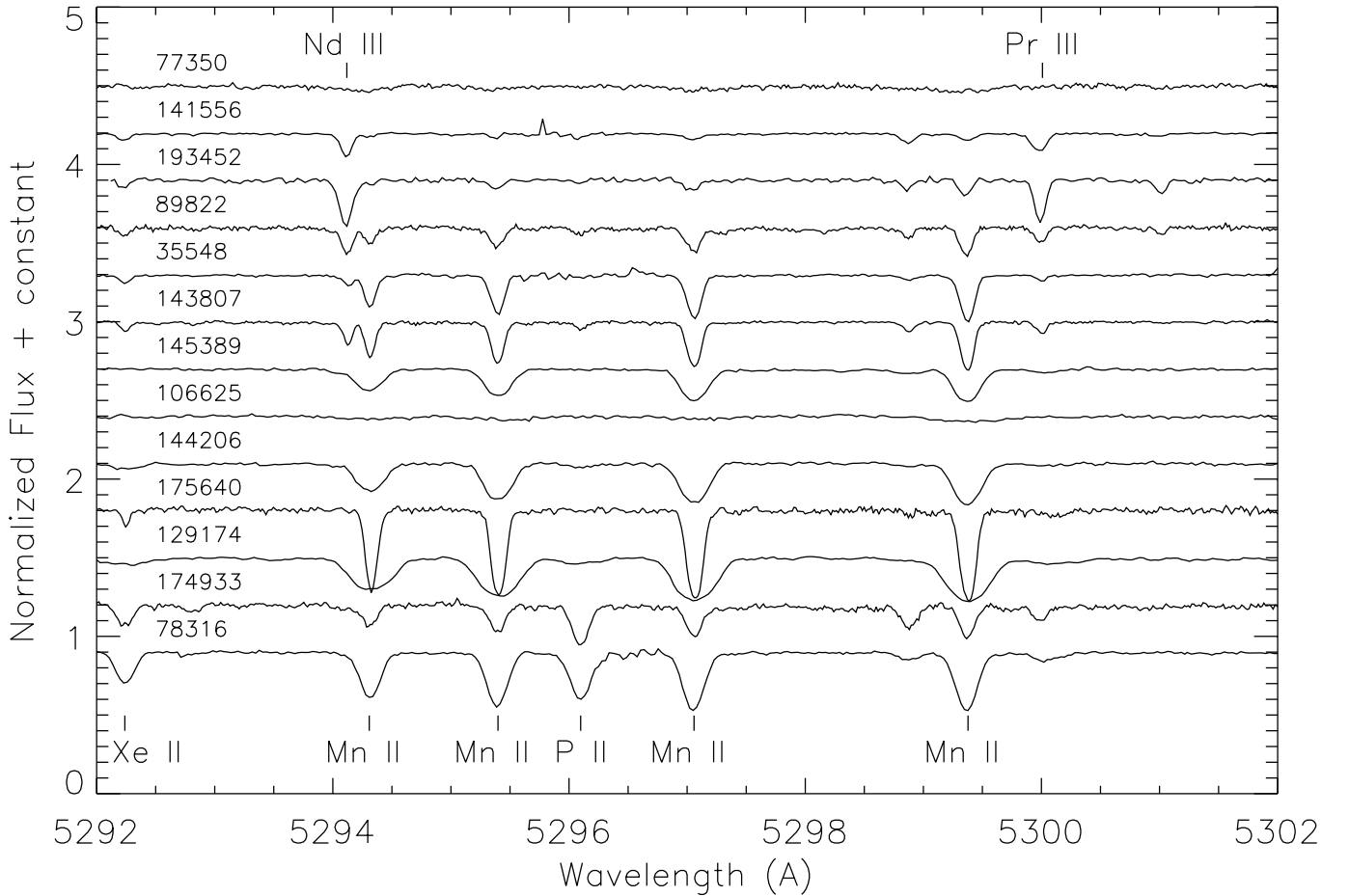
Fig. 2. Spectra of HgMn stars including the Nd III $\lambda 5294$ and Pr III $\lambda 5299$ lines. The stars, identified by their HD numbers, are arranged by effective temperature with the coolest HgMn star on top.

of the Mn II line agrees well with the observed line profile, and the line has therefore been treated as a single component line. The log gf value of the Mn II $\lambda5294$ line presented in the Kurucz database was found to be too small, and was adjusted until the synthetic line profile matched the observed line profile. The Kurucz value of log $gf = -0.037$ was subsequently increased to $+0.563$ to achieve a good fit.

As seen in Table 10, neodymium is, similar to praseodymium, noticeably more enhanced in the cooler HgMn stars than in the hotter ones. This is also illustrated in Fig. 2, where the spectra of the observed HgMn stars are plotted in a region including the Nd III $\lambda5294$ line. The strength of the Nd III line is difficult to assess for the stars with $v \sin i > 5$ km s^{-1}, due to a blend with the aforementioned Mn II line.

Different temperature trends can be seen from the lines of other elements in Fig. 2. The increase in strength of the Mn II lines with effective temperature reflects their known behaviour in HgMn stars (see for instance Smith & Dworetsky 1993). The increase in strength of the P II line in the hotter HgMn stars of our sample is similarly a reflection of the known increase of the phosphorous abundance in HgMn stars with $T_{\text{eff}} > 13\,000$ K (Guthrie 1984). The Xe II line in Fig. 2 is noticeably stronger in the two hottest HgMn stars than in the other observed HgMn stars. This may be a reflection of an abundance increase of xenon towards hotter HgMn stars and/or of the high ionization potential of xenon.

Two of the hotter HgMn stars (HR 6520 and HR 6759) seem to have a similar neodymium enhancement as the cooler stars. These stars have only been observed in a very limited region of the spectrum, with only one Nd III line, the $\lambda6145$ line, being observed. The log gf value of this Nd III line is quite low, and in HR 7245 and HR 6520 the feature is quite weak and the spectrum a little noisy. Therefore it is debatable whether the feature is actually the Nd III line, another unknown line or a noise feature. Other Nd III lines need to be studied in these stars to verify the abundance. There is no question that there is a feature in the spectrum of the hottest HgMn star in our study, HR 6759. If the neodymium abundance in HR 6759 is as high as in the cooler HgMn stars in our study, it could be a sign that this star is related to the magnetic Bp stars, in which the lanthanides typically are greatly enhanced.

The hot-Am stars Sirius, HR 3383 and o Peg, with effective temperatures of approximately 10 000 K, were studied to see if the praseodymium and neodymium abundance enhancement from the Am stars through the cooler HgMn stars is increasing monotonically with effective temperature. In HR 3383 lines from Nd II, Nd III and Pr III were observed, while the limited wavelength coverage of the o Peg and Sirius spectrum made it possible only to observe lines from Nd II. The derived abundance enhancement for praseodymium and neodymium for the three stars were consistent with a 1.0–1.2 dex enhancement (see Table 11), similar to what is observed in cooler Am stars.

Table 11. Abundance of Pr and Nd in the Program stars.

HD	star	T_{eff}	Abundance	
		(K)	Nd	Pr
209625	32 Aqr	7851	2.45	1.60
214994	o Peg	9590	2.70	
72660	HR 3383	9750	2.65	1.85
48915	Sirius	9850	2.65	
77350	ν Cnc	10 400	2.50	2.10
141556	χ Lupi	10 608	3.35	2.80
193452	HR 7775	10 750	4.10	3.68
89822	HR 4072	10 900	3.55	2.85
149121	28 Her	10 908	2.65	2.70
35548	HR 1800	11 050	2.95	2.45
143807	ι CrB	11 250	3.15	2.65
145389	ϕ Her	11 781	2.70	2.40
106625	γ Crv	12 002	2.40	<2.20
144206	υ Her	12 013	2.50	2.25
175640	HR 7143	12 077	<1.90	<1.80
178065	HR7245	12 193	2.80	
186122	46 Aql	12 914	<1.90	<1.90
129174	π Boo A	13 037	<2.50	<2.70
158704	HR6520	13 163	<3.10	
190229	HR 7664	13 240	<1.90	<2.10
174933	112 Her	13 294	<2.40	<2.40
78316	κ Cnc	13 470	<2.30	<2.30
165493	HR6759	13 890	3.50	

6. Discussion

The abundance results for praseodymium and neodymium have been summarized in Table 11. From this table it can be seen that the abundance of neodymium is greater than the abundance of praseodymium in all cases where both abundances have been determined, excluding 28 Her. But since the derived praseodymium abundance was established from one noise affected Pr III line, it is more uncertain in this star. Excluding 28 Her the Nd-Pr abundance difference in the cool HgMn stars varies from 0.3 dex in ϕ Her to 0.7 dex in HR 4072 and ι CrB, which is consistently less than the 0.8 dex difference observed in the Sun (Grevesse et al. 1996) and in our observations of 32 Aqr, Sirius and HR 3383.

It is also noted that for HgMn stars of similar temperature the abundance of neodymium and praseodymium can be significantly different. The previously mentioned trend of the cooler HgMn stars having greater enhancements of praseodymium and neodymium is, however, clearly evident. Because of the generally lower abundance for praseodymium this trend is more readily observable for neodymium.

One of the goals of this study was to investigate the relationship between the Am and the HgMn stars and to establish whether there is evidence that the HgMn and

Am star phenomena are really the same but seen from different effective temperatures. If this is correct one might expect to see a smooth change in the elemental abundances with temperature as, for example, affected by radiative acceleration increasing with temperature. If the abundances observed for the two groups of stars are clearly different, it might be construed as a sign of multiple physical processes (diffusion, rotation, magnetic fields) at work, or a more complicated dependence on effective temperature (diffusion, convection).

The neodymium abundance in Am stars is typically enhanced 1 dex over the solar abundance (see for instance Adelman et al. 1997, 1999). For praseodymium a similar enhancement is usually not sufficient for the optical region Pr II lines to be observable. The solar abundance of praseodymium is 0.8 dex less than the neodymium abundance. Thus the praseodymium abundance has seldom been quoted in abundance analyses of Am stars mostly due to the low abundance. In the cases where Pr II lines have been observed the derived abundance seems to be consistent with a 1 dex enhancement.

For all the HgMn stars with $T_{\rm eff} < 12\,000$ K in our study the neodymium and praseodymium abundances are more than 1.2 dex enhanced, with most of the stars showing a 1.5–2.5 dex enhancement. This large an enhancement clearly distinguishes the cool HgMn stars from the Am stars. The star ν Cnc has a similar neodymium enhancement as the Am stars and its temperature is lower than the HgMn stars studied here. This star has been thought of as an intermediary object between the Am and the HgMn stars (Adelman 1989), and the 1 dex enhancement of neodymium might indicate a closer relation to the Am class of stars.

From the observed abundances of praseodymium and neodymium one can see a temperature regime, roughly between 10 500 and 12 000 K, within which the enhancement of the two elements is noticeably larger than the enhancement in cooler (Am) and hotter (HgMn) non-magnetic CP stars. Here, the term non-magnetic refers to the stars for which magnetic fields are not obvious through the observation of magnetic line broadening or intensification. There are no clear signs of a smooth transition of the praseodymium and neodymium abundance with temperature to and from this temperature regime where the enhancement is pronounced. Instead, it seems like there is a more abrupt change from an enhancement of approximately 1 dex in stars with $T_{\rm eff}$ below 10 500 K, to a 1.5–2.5 dex enhancement in stars with $T_{\rm eff}$ between 10 500 and 12 000 K, and back to an upper limit enhancement of approximately 1 dex in the hotter stars of our group.

The enhancement of certain elements in Am and HgMn stars as well as the depletions of others is postulated to result from diffusive processes active in stellar atmospheres and envelopes. According to the diffusion hypothesis put forward by Michaud (1970), the anomalous abundances are the result of the ion being pushed upwards or brought downwards depending upon whether the radiation pressure is greater or smaller than the gravitational force.

For each ion the diffusion hypothesis can predict abundance anomalies that result from radiation pressure acting through atomic transitions (see for instance Michaud 1975). The calculated radiative force depends on the stellar effective temperature, the atmospheric conditions as well as on the atomic weight of the element and details regarding its atomic structure. Calculations of abundance anomalies are complicated and simplifying assumptions and approximations are made. For most elements the calculated abundance is significantly higher than the observed abundance, which can perhaps be interpreted as other processes within the stellar atmospheres (turbulence) inhibiting diffusion. Calculations to establish the expected abundance enhancement of praseodymium and neodymium have not been made since the atomic physics of these elements and other rare earths is rather poorly known, making the diffusion calculations highly uncertain (Michaud et al. 1976).

Non-magnetic CP stars with $T_{\rm eff} < 10\,000$ K are assumed to arrive on the main sequence with solar-like abundances and their H and He convection zones separated by a radiative zone (Michaud 1986). With time He settles gravitationally which leaves the star with a thin superficial H convection zone above a radiative zone. In the radiative zone elements supported by radiative acceleration are pushed into the convection zone and their abundances are observed enhanced, while elements with radiative force smaller than the gravitational force settle and are observed as depleted. In CP stars with $T_{\rm eff} > 10\,000$ K most of the hydrogen is ionized and no superficial convection zone exists. Instead these stars may have a small He convection zone that dissipates over time as a result of He settling gravitationally. After the He convection zone has disappeared the diffusive separation can go on directly in the stellar atmosphere.

The observed jump in the neodymium and praseodymium abundance at an effective temperature of approximately 10 500 K can perhaps be explained with the disappearance or diminishing of the H convection zone. The observed 1 dex abundance enhancement of praseodymium and neodymium in the Am stars may result from ongoing diffusive processes occurring below the H convection zone, bringing the elements closer to the stellar surface (influence from other processes, such as magnetic buoyancy, may also be contributing to enhanced line strengths). In the cool HgMn stars the lack of a convection zone might cause the elements to rise higher through diffusion than in the Am star atmospheres, with a subsequent increase in the observed abundances.

The apparent discontinuity in the neodymium and praseodymium abundance in the vicinity of the Am-HgMn boundary is similar in nature to the jump observed for the mercury abundance between the hotter Am and the HgMn stars (see for instance Wahlgren et al. 1993, 1998 and Rooke 1999), where the Am stars have a moderate 1.5 dex enhancement of mercury, while the HgMn stars

have a pronounced mercury enhancement ranging between 3.5–6 dex. The larger difference in the mercury abundance between Am and HgMn stars, compared to the difference in praseodymium and neodymium abundance, is possibly a reflection of diffusion acting more efficiently on mercury than on praseodymium and neodymium, something that may be explained by the difference in atomic structure and mass of these elements (see for instance Michaud et al. 1976; Michaud 1987).

After additional elements are investigated for their abundance in stars in the vicinity of the HgMn – Am boundary it may become possible to understand and explain the interplay between atomic properties (structure, mass) and atmospheric processes (diffusion, convection, magnetic fields, mass loss) in these stars. Such investigations would provide tighter constraints for theoretical investigations of atmospheric processes in CP stars.

References

Abt, H. A., & Morrell, N. I. 1995, ApJS, 99, 135

Abt, H. A., & Snowden, M. S. 1973, ApJS, 25, 137

Adelman, S. J. 1987, MNRAS, 228, 573

Adelman, S. J. 1988, MNRAS, 235, 763

Adelman, S. J. 1989, MNRAS, 239, 487

Adelman, S. J. 1992, MNRAS, 258, 167

Adelman, S. J. 1994, MNRAS, 266, 97

Adelman, S. J., Caliskan, H., Kocer, D., & Bolcal, C. 1997, MNRAS, 288, 470

Adelman, S. J., Caliskan, T., Cay, H., et al. 1999, MNRAS, 305, 591

Ahmad, S. A., & Saksena, G. D. 1977, Phys. C, 85, 191

Aikman, G. C. L. 1976, Pub. Dom. Astro. Obs., 14, 379

Aldénius, M. 2001, Master Thesis, Department of Physics, Univ. of Lund

Andersen, T., & Sörensen, G. 1974, Sol. Phys., 38, 343

Andersen, T., Poulsen, O., Ramanujam, P. S., & Petrakiev-Petkow 1975, Sol. Phys., 44, 257

Batten, A. H., Fletcher, J. M., & MacCarthy, D. G. 1989, Pub. Dom. Astro. Obs., 17, 1

Bidelman, W. P. 1966, Abundance Determinations in Stellar Spectra, ed. H. Hubenet (Academic Press: London), IAU Symp., 26, 63

Biémont, E., Garnir, H. P., Palmeri, P., et al. 2001, Phys. Rev. A, in press

Blaise, J. 1957, Thesis, Univ. Paris, 112

Blaise, J., Wyart, J-F., Djerad, M. T., & Ahmed, Z. B. 1984, Phys. Scr., 29, 119

Bolcal, C., Kocer, D., & Adelman, S. J. 1992, MNRAS, 258, 270

Bord, D. J. 2000, A&AS, 144, 517

Brault, J. W., & Abrams, M. C. 1989, OSA Technical Digest Series, vol. 6, Opt. Soc. Am., Washington 110

Corliss, C., & Bozman, U. 1962, NBS Monograph 53, Washington

Cowan, R. D. 1981, The Theory of Atomic Structure and Spectra (Berkeley: Univ. of Californian Press)

Cowley, C. R. 1983, Phys. Scripta, vol. T8, 28

Gerbaldi, M., Floquet, M., & Hauck, B. 1985, A&A, 146, 341

Gorshkov, V. N., & Komarovskii, V. A. 1985, Opt. Spectrosc. (USSR) 58, 561

Grevesse, N., Noels, A., & Sauval, A. J. 1996, Cosmic Abundances, ed. S. S. Holt, & G. Sonneborn (ASP: San Fransisco), ASP Conf. Ser., 99, 117

Guthrie, B. N. G. 1981, 23eme colloque inter. d'Astrophys. Liège, 189

Guthrie, B. N. G. 1984, MNRAS, 206, 85

Guthrie, B. N. G. 1985, MNRAS, 216, 1

Hauck, B., & Mermilliod, M. 1980, A&AS, 40, 1

Hoffleit, D., & Jascheck, C. 1982, The Bright Star Catalogue (New Haven:Yale Univ. Obs.)

Holt, R. A., Scholl, T. J., & Rosner, S. D. 1999, MNRAS, 306, 107, and website http://gandalf.physics.uwo.ca/atomic/

Hubrig, S., Castelli, F., & Wahlgren, G. M. 1999, A&A, 346, 139

Hubrig, S., & Mathys, G. 1994, Workshop on Laboratory and Astronomical High Resolution Spectra, ed. A. J. Sauval, R. Blomme, & N. Grevesse (ASP: Brussels), ASP Conf. Ser., 81, 555

Ilyin, I. 1993, SOFIN User's manual

Ilyin, I. 2000, Ph.D. Thesis, University of Oulu

Ivarsson, S., Litzén, U., & Wahlgren G. M. 2001, Phys. Scripta, in press

King, W. H., Steudel, A., & Wilson, M. 1973, Z. Phys., 265, 207

Kocer, D., Bolcal, C., Inelmen, E., & Adelman, S. J. 1987, A&AS, 70, 49

Kurucz, R. L. 1993a, Synthesis Programs and Line Data, (Kurucz CD-ROM No. 18)

Kurucz, R. L. 1993b, ASP Conf. Ser., 44, 87

Kurucz, R. L., & Avrett, E. H. 1981, Solar Spectrum Synthesis. I. A Sample Atlas from 224 to 300 nm (Smithsonian Astrophys. Obs. Spec. Rept. 391)

Landstreet, J. D. 1998, A&A, 338, 1041

Lane, M. C., & Lester, J. B. 1987, ApJS, 65, 137

Li, Z. S., Norin, J., Persson, A., et al. 1999, Phys. Rev. A, 60, 198

Magazzu, A., & Cowley, C. R. 1986, ApJ, 308, 254

Martin, W. C., Zalubas, R., & Hagan, L. 1978, NSRDS-NBS 60, Washington

Mathys, G., & Cowley, C. R. 1992, A&A, 253, 199

Meggers, W. F, Corliss, C. H., & Scribner, B. F. 1975, NBS Monograph, 145

Michaud, G. 1970, ApJ, 160, 641

Michaud, G. 1975, Physics of Ap-stars, ed. W. W. Weiss, H. Jenkner, & H. J. Wood (Finsterle & CO. KG.: Vienna), IAU Coll., 32, 81

Michaud, G., Charland, Y., Vauclair, S., & Vauclair, G. 1976, ApJ, 210, 447

Michaud, G. 1987, Phys. Scr., Vol. RS5, 66

Moon, T. T., & Dworetsky, M. M. 1985, MNRAS, 217, 305

Nakhate, S. G., Afzal, S. M., & Ahmad, S. A. 1997, Z. Phys. D, 42, 71

Napiwotzki, R., Schoenberner, D., & Wenske, N. 1993, A&A, 268, 6T3

Nielsen, K., & Wahlgren, G. M. 2000, A&A, 356, 146

Nöldeke, G. 1955, Z. Phys., 143, 274

Palmeri, P., Quinet, P., Frémat, Y., Wyart, J-F., & Biémont, E. 2000, ApJS, 129, 367

Perryman, M., et al. 1997, The Hipparcos and Tycho Catalogues, European Space Agency SP-1200 (Noordwijk: ESA)

Proffitt, C. R., Brage, T., Leckrone, D. S., et al. 1999, ApJ, 512, 942

Radick, R., & Lien, D. 1980, AJ, 85, 1053

Renson, P. 1991, Catalogue Général des Étoiles Ap et Am, Institut d'Astrophysique-Université de Liège

Rooke, S. 1999, Master Thesis, Department of Physics, Univ. of Lund

Ryabchikova, T. A., Zakharova, L. A., & Adelman, S. J. 1996, MNRAS, 283, 1115

Ryabchikova, T. A. 1998, Contrib. Astron. Obs. Skalnaté Pleso, 27, 319

Ryabchikova, T. A., Savanov, I. S., Malanushenko, V. P., & Kudryavtsev, D. O. 2001, Astronomy Reports, 45, 382

Schneider, H. 1986, Upper Main Sequence Stars with Anomalous Abundances, ed. C. R. Cowley, M. M. Dworetsky, & C. Mégessier (Reidel: Dordrecht), IAU Coll., 90, 205

Smith, M. A. 1971, A&A, 11, 325

Smith, M. A. 1976, ApJ, 203, 603

Smith, K. C. 1992, Ph.D. Thesis, University of London

Smith, K. C, & Dworetsky, M. M. 1993, A&A, 274, 335

Sugar, J. 1974, J. Res. Nat. Bur. Stds., 78A, 555

Tuominen, I., Ilyin, I., & Petrov, P. 1998, Astrophysics with the NOT, ed. H. Karttunen, & V. Piirola (University of Turku: Turku), 47

Wahlgren, G. M., Leckrone, D. S., Johansson, S., & Rosberg, M. 1993, Peculiar Versus Normal Phenomena in A-Type and Related Stars, ed. M. M. Dworetsky, F. Castelli, & R. Faraggiana (ASP: San Fransisco), ASP Conf. Ser., 44, 121

Wahlgren, G. M., Adelman, S. J., & Robinson, R. D. 1994, ApJ, 434, 349

Wahlgren, G. M. 1996, Model Atmospheres and Spectrum Synthesis, ed. S. J. Adelman, F. Kupka, & W. W. Wiese (ASP: San Fransisco), ASP Conf. Ser., 108, 240

Wahlgren, G. M., & Dolk, L. 1998, Contrib. Astron. Obs. Skalnaté Pleso, 27, 314

Wahlgren, G. M, Dolk, L., Kalus, G., Johansson, S., & Litzén, U. 2000, ApJ, 539, 908

Ward, L., Vogel, O., Arnesen, A., Hallin, R., & Wannstrom, A. 1985, Phys. Scr., 31, 162

White, R. E., Vaughan, (Jr) A. H., Preston, G. W., & Swings, J. P. 1976, ApJ, 204, 131

Wolff, S. C., & Preston, G. W. 1978, ApJS, 37, 371